

ELLIPSOMETRIC AND UV-VIS TRANSMITTANCE ANALYSIS OF
AMORPHOUS SILICON CARBIDE THIN FILMS

A THESIS SUBMITTED TO
THE GRADUATE SCHOOL OF NATURAL AND APPLIED SCIENCES
OF
MIDDLE EAST TECHNICAL UNIVERSITY

BY

ALİ ALKAN GÜLSES

IN PARTIAL FULFILLMENT OF THE REQUIREMENTS
FOR
THE DEGREE OF MASTER OF SCIENCE
IN
PHYSICS

DECEMBER 2004

Approval of the Graduate School of Natural and Applied Sciences.

Prof. Dr. Canan Özgen
Director

I certify that this thesis satisfies all the requirements as a thesis for the degree of Master of Science.

Prof. Dr. Sinan Bilikmen
Head of Department

This is to certify that we have read this thesis and that in our opinion it is fully adequate, in scope and quality, as a thesis for the degree of Master of Science.

Prof. Dr. Bayram Katırcıoğlu
Supervisor

Examining Committee Members

Prof. Dr. İbrahim Günel (METU, PHYS) _____

Prof. Dr. Bayram Katırcıoğlu (METU, PHYS) _____

Assoc. Prof. Dr. Dr. İsmail Atılgan (METU, PHYS) _____

Assoc. Prof. Dr. Dr. Osman Kodolbaş (HU, PHYS) _____

Dr. Barış Akaoğlu _____

I hereby declare that all information in this document has been obtained and presented in accordance with academic rules and ethical conduct. I also declare that, as required by these rules and conduct, I have fully cited and referenced all material and results that are not original to this work.

Name, Last name :

Signature :

ABSTRACT

ELLIPSOMETRIC AND UV-VIS TRANSMITTANCE ANALYSIS OF AMORPHOUS SILICON CARBIDE THIN FILMS

Gülses, Ali Alkan

M.S., Department of Physics

Supervisor: Prof. Dr. Bayram Katircioğlu

December 2004, 81 pages

The fundamentals of the ellipsometry are reviewed in order to point out the strengths and weaknesses of the ellipsometric measurements. The effects of the surface conditions (such as degree of cleanliness, contaminated thin layer, roughness etc...) on the ellipsometric variables are experimentally studied; the optimum procedures have been determined. Hydrogenated amorphous silicon carbide ($a\text{-Si}_{1-x}\text{C}_x\text{H}$) thin films are produced by plasma enhanced chemical vapor deposition (PECVD) technique with a circular reactor, in a way that RF power and carbon contents are taken as variables. These samples are analyzed using multiple angle of incidence ellipsometer and uv-vis spectrometer. These measurements have inhomogeneities in optical constants, such as thicknesses, refractive indices and optical energy gaps along the radial direction of the reactor electrode for different power and carbon contents.

Keywords: PECVD, Amorphous silicon carbide, spectroscopy, ellipsometry, optical constants, inhomogeneity.

ÖZ

AMORF SİLİSYUM KARBÜR İNCE FİMLERİN ELİPSOMETRİK VE MOR ÖTESİ – GÖRÜNÜR BÖLGE OPTİK GEÇİRME ANALİZİ

Gülses, Ali Alkan

Yüksek Lisans, Fizik Bölümü

Tez Yöneticisi: Prof. Dr. Bayram Katırcıoğlu

Aralık 2004, 81 sayfa

Elipsometrik ölçümlerin kuvvetli ve zayıf taraflarına dikkat çekmek için elipsometrinin temelleri gözden geçirildi. Yüzey koşullarının (temizlik derecesi, ince kir tabakası, pürüzlülük vb.) elipsometrik değişkenler üzerindeki etkileri deneysel olarak çalışıldı. Optimum prosedürler belirlendi. Hidrojenlenmiş amorf silisyum karbür ($a\text{-Si}_{1-x}\text{C}_x\text{:H}$) ince filmler, carbon içeriği ve RF gücü değişken alınarak, dairesel elektrodlu plazma destekli kimyasal buhar biriktirme (PECVD) tekniği ile üretilmiştir. Bu örnekler çok açılı elipsometre ve mor ötesi – görünür bölge dalgaboylu spektrometre kullanılarak incelendi. Ölçümlere göre, reaktör elektrodunun merkezinden kenara doğru, farklı güç ve karbon içerikli filmlerin, kalınlıklar, kırıcılık indisleri ve enerji aralıkları gibi optik sabitlerde düzensizlik gösterdiği saptandı.

Anahtar Kelimeler: Amorf silisyum karbür, spektroskopi, Elipsometri, optik sabitler, düzensizlik.

ACKNOWLEDGEMENTS

I wish to thank to Prof. Dr. Bayram Katırcıođlu, Assoc. Prof. Dr. İsmail Atılğan and Dr. Barıř Akaođlu for their guidance, advice and encouragements throughout my work.

TABLE OF CONTENTS

PLAGIARISM.....	iii
ABSTRACT	iv
ÖZ	v
ACKNOWLEDGMENTS.....	vi
TABLE OF CONTENTS	vii
LIST OF TABLES.....	ix
LIST OF FIGURES.....	x
CHAPTER	
1. INTRODUCTION	1
2. THEORETICAL OUTLINE.....	4
2.1 Light as an Electromagnetic Wave.....	4
2.2 Relation of the Extinction Coefficient and the Absorption Coefficient.....	8
2.3 Interaction of Light With Material.....	9
2.4 Brewster Angle.....	11
2.5 Swanepoel's method.....	12
2.6 Polarization of Light.....	17
2.7 Jones Formulation for Polarization.....	19
2.7.1 Introduction.....	19
2.7.2 Jones Vectors.....	19
2.7.3 Jones Matrices.....	21
2.8 Ellipsometry.....	22
2.8.1 Introduction.....	22
2.8.2 Ellipsometry Equations.....	23
2.9 Film-Substrate Systems.....	25

2.9.1	The Single Substrate.....	25
2.9.2	Air-film-Substrate System.....	26
2.9.3	Dependence of ρ on the Film Thickness.....	27
2.10	Multilayer Films.....	28
2.11	Conclusion.....	29
3.	INSTRUMENTATION.....	30
3.1	Plasma System (Plasma Enhanced Chemical Vapor Deposition).....	30
3.1.1	Overview.....	30
3.1.2	Interaction of the Plasma with Substrate.....	32
3.2	UV-Visible Spectrometer (Perkin Elmer Lambda 2S)	35
3.3	The Ellipsometry setup.....	37
3.3.1	Optical Elements.....	37
3.3.2	The Ellipsometer.....	37
3.3.3	Specifications of the Ellipsometer.....	40
3.3.4	Operating Principles.....	43
4.	EXPERIMENTAL STUDIES.....	44
4.1	Optical Absorption in Solids.....	44
4.2	Hydrogenated amorphous silicon carbide ($a\text{-Si}_{1-x}\text{C}_x\text{:H}$) Thin Films.....	48
4.2.1	Structure of the a-Si.....	48
4.2.2	Structure of the a-C.....	49
4.2.3	Structure of the Bonds.....	51
4.2.4	General Structure.....	52
4.3	Delta (Δ) and Psi (Ψ) Simulations in Ellipsometric Measurements.....	54
4.4	Measurements on Glass Substrate.....	56
4.5	Experiments on Silicon Substrate: Cleanliness effect in ellipsometry.....	59
4.6	Optical Measurements on $a\text{-Si}_{1-x}\text{C}_x$ Thin Films.....	62
4.6.1	Production of $a\text{-Si}_{1-x}\text{C}_x\text{:H}$ Thin Films.....	62
4.6.2	Expected Reactions in the plasma environment.....	65
4.6.3	Optical Experiments.....	68
4.6.4	Discussions.....	68
5.	CONCLUSION	78
	REFERENCES.....	80

LIST OF TABLES

TABLE	
4.1	Index values of corning glass at 632 nm..... 58
4.2	Eight different depositions under a pressure of 0.5 Torr at substrate temperature of 250 °C for the following deposition parameters such as relative C ₂ H ₄ concentration (M(C ₂ H ₄)), SiH ₄ (F(SiH ₄)) and C ₂ H ₄ (F(C ₂ H ₄)) flow rates and power density (P). The letters “lp” and “hp” denote films grown at low and high powers, respectively. Carbon content increases as the sample number increases. Also the deposition times and x value for the a-Si _{1-x} C _x :H are shown..... 63

LIST OF FIGURES

FIGURE

2.1	Light ray (a) entering medium(1) from medium (0), (b) entering the slab of medium(1) from medium (0).....	9
2.2	r_p and r_s versus angle of incidence, for $n_2 = 1.5$ and $n_1 = 1$. r_p becomes zero at the brewester angle which is about 56 degrees.....	12
2.3	Light enters the air-film-substrate system at zero angle of incidence.....	14
2.4	Graph of the eq. (2.34). Ripples are caused by interference effects. Absorption reduces the transmittance as the wavelength decreases.....	14
2.5	Electric vector rotates making an ellipse that principal axis makes an angle θ with the x axis. ellipticity angle ϵ is equal to $\arctan(b/a)$. And amplitude is A...	18
2.6	Oscillation direction of a wave.....	21
3.1	Capacitively coupled radio frequency discharge.....	32
3.2	PECVD system which is used in the production of thin films [15].....	33
3.3	Gas cabinet system in the PECVD system [15].....	34
3.4	Diagram of the optical path of the Perkin-Elmer Lambda 2 spectrometer.....	36
3.5	Optical setup of photometric Ellipsometry.....	38
3.6	Principles of ellipsometric measurement.....	39
3.7	Ellipsometer setup.....	42
3.8	Ellipsometer before measurement. For calibration puposes, transmitter and receiver units have to be aligned before measurement.....	43

4.1	Schematic diagram of the density of states in amorphous semiconductors.....	46
4.2	Electron configuration of Si atom in ground state.....	48
4.3	Electron configuration of Si atom in case of sp^3 hybridization.....	48
4.4	Electron configuration of C atom.....	49
4.5	Carbon atom (a) Electron configuration in sp^3 hybridization, (b) bonding sketch where all the bonds are σ	50
4.6	Carbon atom (a) Electron configuration in sp^2 hybridization, (b) bonding sketch where all the bonds are σ except for the dashed line which is actually a π bond.....	50
4.7	Carbon atom (a) Electron configuration in sp^1 hybridization, (b) bonding sketch where all the bonds are σ except for the dashed lines which are the π bonds.....	51
4.8	Carbon atom bonding structure (a) four σ bonds, (b) carbon atoms are connected by one σ and one π bond, (c) p_y and p_z orbitals form π bonds.....	52
4.9	Schematic energy band diagram of a-C:H.....	52
4.10	Schematic electronic band structure of amorphous carbons.....	53
4.11	Sample del., ψ vs ang. of inc. curve for (a) ideally non-absorbing, (b) weakly absorbing bulk semiconductor (such as silicon).....	55
4.12	Matlab is used to make the simulation. Effect of increasing extinction coefficient is shown. Solid line represents the film with $n=2.6$ and $k=0.4$, while dashed line represents $n = 2.6$ and $k = 0.8$. Thicknesses are 400 nm. Substrates are assumed to be silicon.....	56
4.13	ψ and δ versus angle of incidence curves (a) for bare glass, (b) for band-sticked glass.....	57
4.14	δ and ψ versus Angle of incidence for silicon slab obtained from (a) First measurement, (b) Second measurement. A cleaning procedure is applied before measurement. (c) third measurement. Double cleaning procedure is applied before.....	60

4.15	Comparison of the delta vs Angle of incidence curves for double-cleaned and double-cleaned + oxide free silicon. The change in psi is indistinguishable, therefore it is not shown in the graph.	61
4.16	A series of glass substrates lying on the bottom electrode of the PECVD reactor plasma medium.....	64
4.17	Sketch of the plasma system. Radius is 12 cm. But because the samples are placed 0.5 cm. from the edge, in calculations and graphs radius is taken as 11.5 cm. [13].....	65
4.18	Thickness values from transmittance found by (a) Using the method of Swanepoel for low power. (b) Using the method of Swanepoel for high power. (c) Using numerical techniques for low power and (d) Using numerical techniques for high power. Note that, circles, squares, triangles and diamonds, correspond to increasing carbon contents, respectively. Radial distance of about 0 cm corresponds to the edge of the bottom electrode whereas that of about 11.5 cm corresponds to the center of the electrode.....	69
4.19	(a) Deposition rates, obtained from transmittance (empty markers) and ellipsometry (full markers) measurements, of samples 0lp, 2lp, 5lp and 7lp, denoted by circles, squares, triangles and diamonds, respectively. (b) Deposition rates, obtained from transmittance (empty markers) and ellipsometry (full markers) measurements, of samples 0hp, 2hp, 5hp and 7hp, denoted by circles, squares, triangles and diamonds, respectively. Radial distance of about 0 cm corresponds to the edge of the bottom electrode whereas that of about 11.5 cm corresponds to the center of the electrode.....	71

4.20	(a) Refractive indices, obtained from transmittance (empty markers) and ellipsometry (full markers) measurements, of samples 0lp, 2lp, 5lp and 7lp, denoted by circles, squares, triangles and diamonds, respectively. (b) Refractive indices, obtained from transmittance (empty markers) and ellipsometry (full markers) measurements, of samples 0hp, 2hp, 5hp and 7hp, denoted by circles, squares, triangles and diamonds, respectively. Radial distance of about 0 cm corresponds to the edge of the bottom electrode whereas that of about 11.5 cm corresponds to the center of the electrode.....	74
4.21	E ₀₄ values as a function of radial distance of the bottom electrode, obtained from transmittance measurements of films (a) 0lp, 2lp, 5lp and 7lp, denoted by circles, squares, triangles and diamonds, respectively. (b) 0hp, 2hp, 5hp and 7hp, denoted by circles, squares, triangles and diamonds, respectively. Tauc optical gaps E _g as a function of radial distance of the bottom electrode obtained from transmittance measurements of films (c) 0lp, 2lp, 5lp and 7lp, denoted by circles, squares, triangles and diamonds, respectively and (d) 0hp, 2hp, 5hp and 7hp, denoted by circles, squares, triangles and diamonds, respectively. Radial distance of about 0 cm corresponds to the edge of the bottom electrode whereas that of about 11.5 cm corresponds to the center of the electrode.....	76
4.22	E ₀₄ versus carbon content for (a) low power (b) high power for the same position in the reactor which is 10 cm from the edge.....	77

CHAPTER 1

INTRODUCTION

Modern microelectronics technology is able to reduce the size of both circuit components and the circuit itself below submicron, leading to ULSI (ultra large scale integration). Due to definite human dimensions, some devices can not be minimized further, in order to be used for human- machine interfaces. Some of these devices which are constituted by the so-called large area electronics, can be counted as electronic displays, scanners, solar cells, etc... For such large area, thin solid film materials are used to produce electronic structures.

Silicon is widely preferred in microelectronics industry due to its stable natural oxide. In optoelectronic applications the crystalline silicon remain very mediocre due to its poor optical properties. Hydrogenated amorphous silicon (a-Si-H) with improved optical properties has extended the use of silicon towards optoelectronic field. In this respect, pure amorphous silicon (a-Si) is not suitable due to existence of huge number of dangling bonds, creating a high density of deep states, distributed around the middle of the pseudogap. These defects are always dominant over the doping effects of any dopant foreign atoms by capturing their extra carriers.

In hydrogen silicon alloy (a-Si:H), hydrogen, passivating the majority of the above mentioned dangling bonds (DBs), reduces the density of deep local states. Therefore, makes doping possible. Consequently p-n or p-i-n junctions and circuits based on these building stones can be fabricated.

It is well known that the energy gap is one of the main parameters determining the material optical application. In this respect, the energy gap of

crystalline silicon (1.12 eV at 300K) is shifted from near infrared to visible region for a-Si:H. Moreover, apart from hydrogen, alloying of amorphous silicon with various elements such as Sn, Ge, C, N, O etc... creates a family of hydrogenated amorphous materials whose optical energy gap can be continuously modulated from infrared to UV region. An example of this family is hydrogenated amorphous silicon carbide (a-Si_{1-x}-C_x:H) whose optical gap may be modulated from that of a-Si:H (1.8eV) to amorphous carbon (a-C:H) by adjusting carbon content from $x = 0$ to $x = 1$.

Hydrogenated amorphous silicon carbide (a-Si_{1-x}-C_x:H) thin films are produced using the plasma enhanced chemical vapour deposition (PECVD) technique in different concentrations of carbon gas supply and different powers. Industrial applications require high deposition rates over large areas (35 cm x 45 cm or more for flat screen applications) and a uniformity in layer thickness to better than $\pm 5\%$ for flat screens and about $\pm 10\%$ for solar cells [1].

Spectrometer (at zero angle of incidence) and (single wavelength) ellipsometer are used in the analysis. Spectrometer is a device that uses the unpolarized radiation to illuminate the sample. Intensities of transmitted beams are measured as a function of wavelength. On the other hand, in ellipsometry, polarized radiation is used and both intensity and phase of the reflected beam at multiple angle of incidence are measured to reach the optical constants.

In this work, firstly the theoretical background on electromagnetic waves (EM) and their interaction with matter are given. Then some experimental systems are introduced. Chapter 4 includes experiments, related to optical measurements on surfaces especially inhomogeneities of series of a-Si_{1-x}-C_x:H thin films along the radial direction of the PECVD electrode.

Optical energy gaps are evaluated in addition to optical constants and thicknesses of amorphous Si-C thin films. More than one technique is used to handle the existing data for thickness calculations. One of the techniques involves obtaining

information from the transmission spectrum. And the other is a numerical technique that necessitates computer software to be performed. After all the data are obtained, results are evaluated in the light of literature, and the discussion is made about the effect of power and carbon content on properties of the films, which may allow more appropriate thin film production in the future.

CHAPTER 2

THEORETICAL OUTLINE

2.1 Light as an Electromagnetic Wave

Light is an Electromagnetic (EM) wave. An electromagnetic wave is an energy flow in space consisting of electric and magnetic fields. That electromagnetic disturbance that propagates through space as a wave may be monochromatic, that is characterized by a single wavelength, or polychromatic, in which case it is represented by many wavelengths, either discrete or continuous. The distribution of energy among the various constituent waves is called the spectrum of the radiation and various regions of the spectrum are referred to by particular names, such as radio waves, ultraviolet radiations, visible radiations to which the human eye is sensitive only, etc...

EM waves are described by four fundamental equations. These are the Maxwell's equations. Each of these equations represents a generalization of certain experimental observations. They can be written compactly, in any medium, as

$$\vec{\nabla} \times \vec{H} = \vec{J} + \frac{\partial \vec{D}}{\partial t} \quad (2.1a) \qquad \vec{\nabla} \cdot \vec{D} = \rho \quad (2.1c)$$

$$\vec{\nabla} \times \vec{E} = -\frac{\partial \vec{B}}{\partial t} \quad (2.1b) \qquad \vec{\nabla} \cdot \vec{B} = 0 \quad (2.1d)$$

\vec{E} is the electric field vector, \vec{D} is the electric displacement vector, \vec{B} is the magnetic field vector, \vec{H} is the magnetic intensity vector, \vec{J} is the current density vector and finally ρ represents the volume charge density.

In dielectrics, during the interaction with light, electromagnetic nature of light produces dipole moments by making the atoms polarized. The degree of polarization is expressed as polarization vector \vec{P} , which is defined as the dipole moments per unit volume. In dielectrics the following equation holds

$$\vec{D} = \epsilon\vec{E} = \epsilon_0\vec{E} + \vec{P} \quad (2.2)$$

In matter, similar to the polarization effects due to the electric field of the radiation, magnetic effects, caused by the magnetic nature of light, have to be considered. In the presence of a magnetic field, matter becomes magnetized due to the small current loops in atoms. The degree of magnetization is expressed as magnetization vector \vec{M} , which is defined as magnetic dipole moment per unit volume. Magnetic intensity vector is used in the definition of magnetized media, and defined as

$$\vec{H} = \frac{1}{\mu}\vec{B} = \frac{1}{\mu_0}\vec{B} - \vec{M} \quad (2.3)$$

In order to find a general wave equation in space applicable to any medium, the curl of both sides of the eq. (2.1b) is taken, and with the help of eqs. (2.2), (2.3) and the relation $\vec{J} = \sigma\vec{E}$, wave equation for the electric field is obtained.

$$\nabla^2\vec{E} - \epsilon\mu\frac{\partial^2\vec{E}}{\partial t^2} - \sigma\mu\frac{\partial\vec{E}}{\partial t} = 0 \quad (2.4)$$

In the same manner, the wave equation for the magnetic field can be derived as [2]

$$\nabla^2 \vec{H} - \varepsilon\mu \frac{\partial^2 \vec{H}}{\partial t^2} - \sigma\mu \frac{\partial \vec{H}}{\partial t} = 0 \quad (2.5)$$

In order to solve the eq. (2.4), first consider the time dependence is in exponential form,

$$\vec{E}(r,t) = \vec{E}(r)e^{i\omega t}$$

Secondly, consider the propagation direction is only along the z-axis. Then the wave equation for electric field reduces to

$$\frac{\partial^2 E(z)}{\partial z^2} = -\kappa^2 E(z) \quad (2.6)$$

κ is defined as the propagation constant and it is seen to be equal to $\kappa^2 = \varepsilon\mu\omega^2 - i\sigma\mu\omega$. Its direction denotes the propagation direction of radiation. Its magnitude is $\kappa = 2\pi/\lambda$. κ can also be defined as,

$$\kappa = N \frac{\omega}{c} \quad (2.7)$$

N is the complex refractive index of the medium. For vacuum $N = 1$, for air $N = 1.0003$. And it can be taken as 1. Refractive index is composed of real and imaginary parts.

$$N = n - ik \quad (2.8)$$

n is called index of refraction, k is called extinction coefficient. They are always real and positive. They depend on the wavelength and this wavelength dependence may be approximated by Cauchy's formula [3]. By using eqs. (2.7) and (2.8), κ may be expressed as

$$\kappa^2 = \varepsilon\mu\omega^2 - i\sigma\mu\omega = (n - ik)^2 \frac{\omega^2}{c^2} \quad (2.9)$$

Equating the real and imaginary parts, the dependence of the n and k to the material internal properties can be found as

$$n = \sqrt{\frac{1}{2} \left[\frac{\varepsilon\mu}{\varepsilon_0\mu_0} + \sqrt{\left(\frac{\varepsilon\mu}{\varepsilon_0\mu_0}\right)^2 + \left(\frac{\sigma\mu}{\omega\varepsilon_0\mu_0}\right)^2} \right]} \quad (2.10)$$

$$k = \sqrt{\frac{1}{2} \left[-\frac{\varepsilon\mu}{\varepsilon_0\mu_0} + \sqrt{\left(\frac{\varepsilon\mu}{\varepsilon_0\mu_0}\right)^2 + \left(\frac{\sigma\mu}{\omega\varepsilon_0\mu_0}\right)^2} \right]} \quad (2.11)$$

returning to the differential eq. (2.6) the solution is easily found to be, $\vec{E} = \vec{E}_0(z)e^{\pm i\kappa z}$, then the general solution of eq. (2.4) is found by selecting the negative solution for the wave propagating to the increasing z as

$$\vec{E}(z, t) = \vec{E}_0 e^{i(\omega t - \kappa z)} \quad (2.12)$$

where propagation constant κ is a complex number. In a nonabsorptive (dielectrics) medium the conductivity is zero, from eq. (2.11), k is zero and the wave exhibits an oscillatory character without decreasing in amplitude, and can also be written as

$$\vec{E}(z, t) = \vec{E}_0 \cos(\omega t - \kappa z) \quad (2.13)$$

In three dimensions z has to be replaced with r . From the Maxwell's equations, it can be shown that the vectors $\vec{\kappa}$, \vec{E} and \vec{B} form a right-handed orthogonal set. Then it can be said that EM waves are transverse. The relationship between these three orthogonal vectors is,

$$\vec{B} = \frac{n}{c} \frac{\vec{\kappa}}{|\vec{\kappa}|} \times \vec{E} \quad (2.14)$$

After defining an electromagnetic wave, electric field, magnetic field and optical parameters n and k , a connection can be made between optical parameters and measurable quantities. Section 2.2 introduces the relation between the absorption in the matter and extinction coefficient k .

2.2 Relation between the Extinction and the Absorption Coefficients

Absorption is an intrinsic property of materials and it plays a crucial role in manufacturing optoelectronic devices. Absorption coefficient α is an indicator of the absorption in the medium and is related to extinction coefficient. Consider a light wave in the z-direction. Its intensity (I) decreases due to the absorption in the medium, and it is expressed as,

$$I(z) = I_0 e^{-\alpha z} \quad (2.15)$$

where I_0 is the initial intensity and α is the absorption coefficient. Let's put eq. (2.7) and (2.8) in (2.12) to obtain,

$$\vec{E}(z, t) = E_0 e^{i\omega t} e^{-in\frac{\omega}{c}z} e^{-k\frac{\omega}{c}z} \quad (2.16)$$

$$I(z) = |\vec{E}(z)|^2 = E_0^2 e^{-2k\frac{\omega}{c}z} \quad (2.17)$$

Using the equality of eq. (2.15) and (2.17), the relation between α and k can be found as

$$\alpha = 2k \frac{\omega}{c} \quad (2.18)$$

In practical point of view, the extinction coefficient is directly obtained from measurements, and then absorption coefficient which is used in band gap energy calculations, is evaluated by using the above relation.

2.3 Interaction of Light With Material

When light passes from one medium to another some of the beam is reflected back and some is transmitted. Consider an EM wave incident on a medium of refractive index N_1 with the angle of incidence θ_0 from the medium of refractive index N_0 (Figure 2.1(a)), it is reflected with θ_0 and refracted with θ_1 according to Snell's laws. To determine the amplitudes of the reflected and transmitted beams, we define (Fresnel) coefficients relating the amplitude of the incoming beam to reflected and transmitted beams.

$$r = \frac{E_{ref}}{E_{inc}} \quad \text{and} \quad t = \frac{E_{trans}}{E_{inc}} \quad (2.19)$$

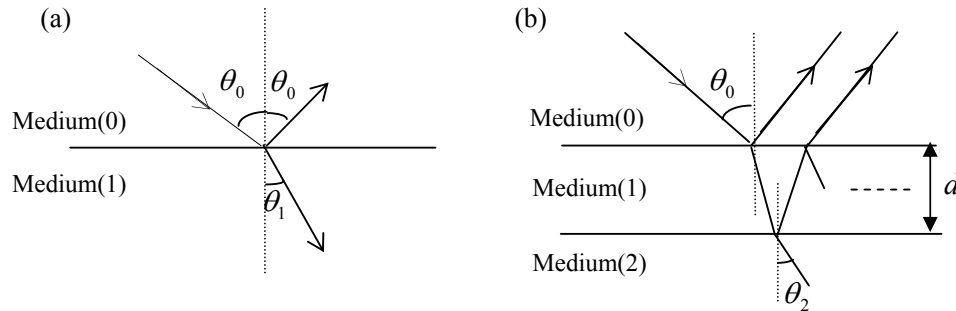


Figure 2.1 Light ray (a) entering medium(1) from medium (0), (b) entering the slab of medium(1) from medium (0).

Then with the help of boundary conditions which express that the tangential components of \vec{E} and \vec{H} fields are continuous when passing one medium to another, the reflection and transmission coefficients can be found. For transverse electric (TE) waves, in which the electric vector is perpendicular to the plane of incidence, these coefficients are equal to,

$$r_{01,s} = \frac{N_0 \cos \theta_0 - N_1 \cos \theta_1}{N_0 \cos \theta_0 + N_1 \cos \theta_1} \quad (2.20)$$

$$t_{01,s} = \frac{2N_0 \cos \theta_0}{N_0 \cos \theta_0 + N_1 \cos \theta_1} \quad (2.21)$$

and, for transverse magnetic (TM) waves, in which the electric vector is parallel to the plane of incidence, it is found that,

$$r_{01,p} = \frac{N_1 \cos \theta_0 - N_0 \cos \theta_1}{N_1 \cos \theta_0 + N_0 \cos \theta_1} \quad (2.22)$$

$$t_{01,p} = \frac{2N_0 \cos \theta_0}{N_1 \cos \theta_0 + N_0 \cos \theta_1} \quad (2.23)$$

In these definitions, the subscript ‘p’ denotes plane polarized electric vector which implies that the magnetic field must be transverse (TM), and the subscript ‘s’ denotes perpendicularly polarized electric vector (TE).

If the system consists of a slab of material bounded on either side by two different semi-infinite medium (Figure 2.1(b)) , the reflection coefficients are found as;

$$r_{total} = r_{01} + t_{01}t_{10}r_{12}e^{-i2\beta} + t_{01}t_{10}r_{10}r_{12}^2e^{-i4\beta} + t_{01}t_{10}r_{10}^2r_{12}^3e^{-i6\beta} + \dots \quad (2.24)$$

From the infinite series, the reflection and transmission coefficients are calculated.

$$r_{p,total} = \frac{r_{01p} + r_{12p} e^{-2i\beta}}{1 + r_{01p} r_{12p} e^{-2i\beta}} \quad , \quad r_{s,total} = \frac{r_{01s} + r_{12s} e^{-2i\beta}}{1 + r_{01s} r_{12s} e^{-2i\beta}} \quad (2.25)$$

$$t_{p,total} = \frac{t_{01p} t_{12p} e^{-i\beta}}{1 + r_{01p} r_{12p} e^{-2i\beta}} \quad , \quad t_{s,total} = \frac{t_{01s} t_{12s} e^{-i\beta}}{1 + r_{01s} r_{12s} e^{-2i\beta}} \quad (2.26)$$

where $\beta = 2\pi \left(\frac{d}{\lambda} \right) \cos \theta_1$, with d is slab thickness. The reflectance (R) is defined as the intensity ratio of the reflected and incoming waves. The transmittance (T) is defined as the intensity ratio of the transmitted and incoming wave. In terms of Frensel coefficients, they are shown to be

$$R = r^2 \quad \text{and} \quad T = \frac{N_2 \cos \theta_2}{N_0 \cos \theta_0} t^2 \quad (2.27)$$

2.4 Brewster Angle

Brewster Angle is a special angle in optics. Its speciality comes from the fact that at a specific angle θ_B the p-component of the reflected wave becomes extinguished (Figure 2.2), and that specific angle is called Brewster's angle, which is in general different for each material. Eq. (2.22) can be written as,

$$r_p = \frac{\tan(\theta_0 - \theta_1)}{\tan(\theta_0 + \theta_1)} \quad (2.28)$$

when $\theta_0 + \theta_1 = \pi/2$, denominator becomes infinity, and r_p is equal to zero for a dielectric matter and has a non-zero minimum value for an absorbing surfaces, although not zero. Using snell's law ($N_1 \sin \theta_1 = N_0 \sin \theta_0$) and the requirement that $\theta_B + \theta_1 = \pi/2$, one can obtain the relation for Brew ster angle

$$\tan \theta_B = \frac{n_1}{n_0} \quad (2.29)$$

Therefore only the indices of mediums are enough for calculation. The property of vanishing one component of the electric field is exploited in optical instruments, such as Polaroid sunglasses.

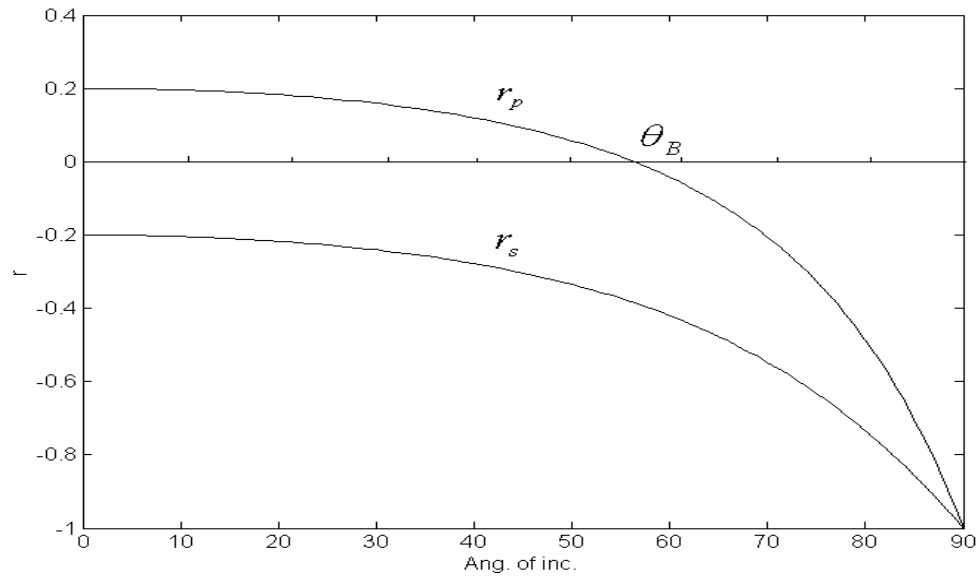


Figure 2.2 r_p and r_s versus angle of incidence, for $n_2 = 1.5$ and $n_1 = 1$. r_p becomes zero at the Brewster angle which is about 56 degrees.

2.5 Swanepoel's Method

In this section, a method is proposed to determine the thickness of a thin film from the interference fringes of the transmission spectrum at zero angle of incidence [4]. Consider a film of thickness d and index $N = n - ik$ on a transparent substrate (Figure 2.3). We need to know the transmittance with taking into account all reflections from the three interfaces.

Considering the thick substrate alone, the coherence length of the light beam is small compared with the material thickness then phase relationship between multiply transmitted rays becomes random and the interference effect disappears [5].

When the light of intensity I_0 is incident on the bare substrate multiple reflections and transmissions are added to give the total intensity of the transmitted light, I_{Total} . The transmittance and reflectance on two surfaces of the substrate is found to be equal from fresnel coefficients. With the help of infinite series and the relation, $T + R = 1$, total transmitted intensity can be found as,

$$I_{Total} = I_0T^2 + I_0T^2R^2 + I_0T^2R^4 \dots = I_0(1-R)^2[1 + R^2 + R^4 \dots] \quad (2.30)$$

$$\frac{I_{Total}}{I_0} = T_{total} = \frac{1-R}{1+R} \quad (2.31)$$

with the help of eqs.(2.20) [or (2.22)] and (2.27) at zero angle of incidence, for bare substrate, the equation for total transmittance becomes,

$$T_{total} = \frac{2n_s}{n_s^2 + 1} \quad (2.32)$$

$$n_{sub} = \frac{1}{T_{total}} + \sqrt{\frac{1}{T_{total}^2} - 1} \quad (2.33)$$

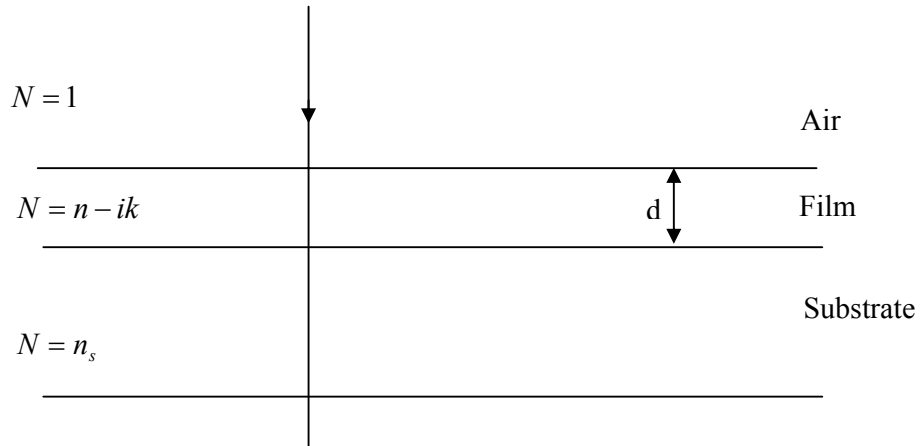


Figure 2.3 Light beam enters the air-film-substrate system at zero angle of incidence.

The transmittance spectrum for Figure 2.3 is plotted in Figure 2.4.

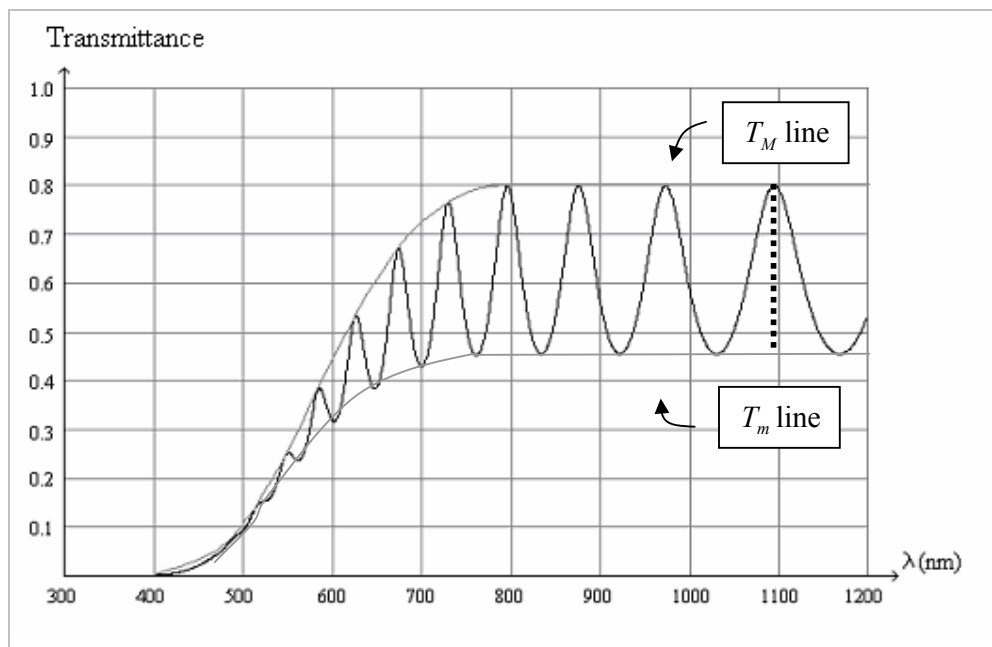


Figure 2.4 Graph of the eq. (2.34). Fringes are caused by interference effects. Absorption reduces the transmittance as the wavelength decreases.

After finding the substrate index, film index and thickness are calculated. For that reason, first transmittance should be formulated. Transmittance in that case can be found by considering the zero interference effect in substrate, taking into account multiple reflections from surfaces and using Fresnel coefficients. In

addition, an assumption can be made on the extinction coefficient k . It can be taken as zero wherever its square enters the equations. Finally its obtained that [4];

$$T_{Total} = \frac{Ax}{B - Cx \cos \varphi + Dx^2} \quad (2.34)$$

where,

$$A = 16n^2n_s \quad (2.35a)$$

$$D = (n-1)^2(n-n_s^2) \quad (2.35d)$$

$$B = (n+1)^3(n+n_s^2) \quad (2.35b)$$

$$\varphi = \frac{4\pi nd}{\lambda} \quad (2.35e)$$

$$C = 2(n^2-1)(n^2-n_s^2) \quad (2.35c)$$

$$x = e^{-\alpha d} \quad (2.35f)$$

The condition for constructive interference is,

$$2nd = m\lambda \quad (m = 0,1,2..) \quad (2.36)$$

Then for $\varphi = 2m\pi$ the transmittance reaches its maximum. Using eq. (2.35e), eq. (2.34) becomes,

$$T_M = \frac{Ax}{B - Cx + Dx^2} \quad (2.37)$$

The condition for destructive interference is,

$$2nd = (m + \frac{1}{2})\lambda \quad (m = 0,1,2..) \quad (2.38)$$

Then for $\varphi = (2m+1)\pi$ the transmittance reduces its minimum Using eq. (2.35e), eq. (2.34) becomes

$$T_m = \frac{Ax}{B + Cx + Dx^2} \quad (2.39)$$

Expressions (2.37) and (2.39) lead to

$$\frac{1}{T_M} - \frac{1}{T_m} = \frac{2C}{A} \quad (2.40)$$

The envelopes of T_M and T_m are also plotted in Figure 2.4. Finally substituting eq. (2.35) into (2.40) and solving for n yields,

$$n = \sqrt{\chi + \sqrt{\chi^2 - n_s^2}} \quad (2.41)$$

where $\chi = 2n_s \frac{T_M - T_m}{T_M T_m} + \frac{n_s^2 + 1}{2}$

If different wavelengths are used in eqs. (2.36) and (2.38), thickness d can be found, for an adjacent maximum and minimum.

$$d = \frac{\lambda_1 \lambda_2}{4(\lambda_1 n_2 - \lambda_2 n_1)} \quad (2.42)$$

Lastly, absorption coefficient can be deduced from eqs.(2.37) and (2.35f) as,

$$\alpha = -\frac{1}{d} \ln \left(\frac{\eta - \sqrt{[\eta^2 - (n^2 - 1)^3 (n^2 - s^4)]}}{(n - 1)^3 (n - s^2)} \right) \quad (2.43)$$

where $\eta = \frac{8n^2 s}{T_M} + (n^2 - 1)(n^2 - s^2)$.

2.6 Polarization of Light

Most of the light sources emit unpolarized light, in which all the electric vectors in the beam randomly oriented in space. If we consider a wave traveling along the z direction, the \vec{E} vector, which is perpendicular to the propagation direction must be in the x - y plane and it can be visualized as having two components one is parallel to x -axis the other is parallel to y -axis. Total field at the position $z = 0$ can be written as,

$$\vec{E}(0,t) = E_x \hat{x} + E_y \hat{y} \quad (2.44)$$

$$\vec{E}(0,t) = E_{x0} \cos(\omega t + \delta_x) \hat{x} + E_{y0} \cos(\omega t + \delta_y) \hat{y} \quad (2.45)$$

With phase differences δ_x and δ_y for x and y component respectively.

In general, components of a light wave have arbitrary phase. Therefore the resultant electric vector traces an ellipse in the x - y plane (Figure 2.5). From eq. (2.45), an equation for an ellipse can be obtained [6].

$$\left(\frac{E_x}{E_{x0}}\right)^2 + \left(\frac{E_y}{E_{y0}}\right)^2 - 2\left(\frac{E_x E_y}{E_{x0} E_{y0}}\right) \cos(\delta_x - \delta_y) = \sin^2(\delta_x - \delta_y) \quad (2.46)$$

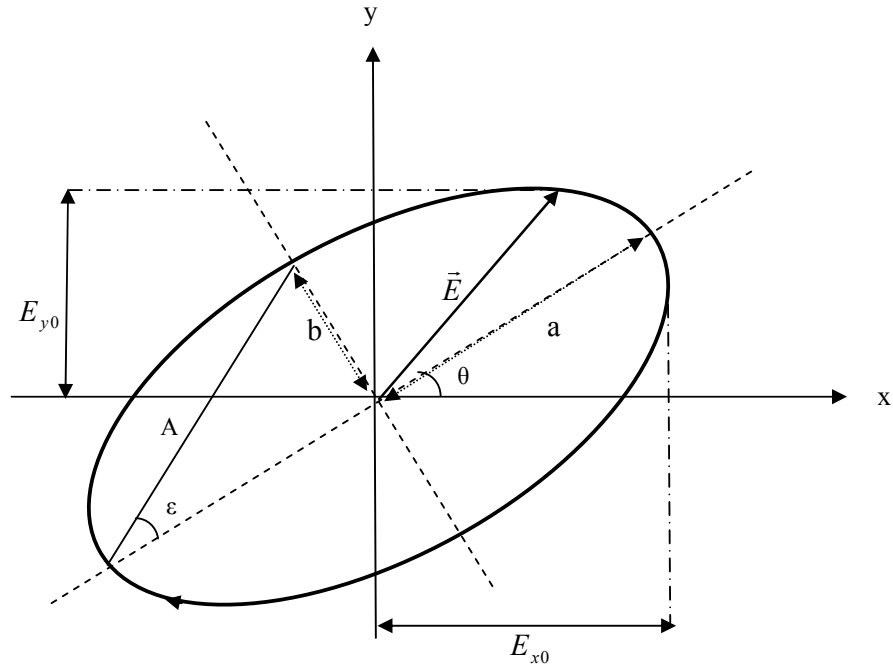


Figure 2.5 Electric vector rotates making an ellipse that principal axis makes an angle θ with the x axis. ellipticity angle ϵ is equal to $\arctan(b/a)$. And amplitude is A.

If the phase difference $(\delta_x - \delta_y)$ is equal to $\frac{\pi}{2}$, the resulting polarization is elliptical but this time principal axis of the ellipse coincides with the x and y axis. Then $a = E_{x0}$, $b = E_{y0}$. Eq.(2.46) reduces to

$$\left(\frac{E_x}{E_{x0}}\right)^2 + \left(\frac{E_y}{E_{y0}}\right)^2 = 1 \quad (2.47)$$

If the two vibrations are in phase or opposite-phase $(\delta_x - \delta_y = 0, \pm \pi)$, then eq. (2.46) gives a straight line equation with a slope of E_{y0}/E_{x0} . which implies a linear polarization as it is stated below.

$$E_y = \pm E_x \frac{E_{y0}}{E_{x0}} \quad (2.48)$$

Linearly polarized wave also-called plane polarized wave can easily be obtained by making ordinary light pass through the polarizer. When light passes through a device that contains optical elements, sometimes it is hard to trace the polarization state. Therefore a new method is needed to handle multiple optical elements.

2.7 Jones Formulation for Polarization

2.7.1 Introduction

In order to simplify the calculations, Jones matrix formulation may sometimes be useful. In this formulation, electric and magnetic fields are represented by 2x1 vectors. On the other hand, optical instruments, involving transmission and reflection, are represented by 2x2 matrices, and overall effect can be calculated by multiplying these matrices. When the wave exit from the optical system, its components are changed according to this overall system matrix.

2.7.2 Jones Vectors

The Electric vector of a monochromatic plane wave propagating to the z-direction has a mathematical form of $\vec{E} = E_{x0} e^{i(\omega t - kz + \delta_x)} \hat{x} + E_{y0} e^{i(\omega t - kz + \delta_y)} \hat{y}$. It can also be described with the help of a matrix as

$$\vec{E} = \begin{bmatrix} E_{x0} e^{i(\omega t - kz + \delta_x)} \\ E_{y0} e^{i(\omega t - kz + \delta_y)} \end{bmatrix} = e^{i(\omega t - kz)} \begin{bmatrix} E_{x0} e^{i\delta_x} \\ E_{y0} e^{i\delta_y} \end{bmatrix} \quad (2.49)$$

Both temporal and spatial dependences can be suppressed for simplification, and can be recovered in case of need. Therefore electric vector can simply be denoted as

$$\vec{E} = \begin{bmatrix} E_x \\ E_y \end{bmatrix} \quad (2.50)$$

where $E_x = E_{x0} e^{i\delta_x}$ and $E_y = E_{y0} e^{i\delta_y}$. This is the Jones vector of an electric field.

To find the intensity of the wave, Jones vector of the electric field has to be multiplied with the Hermitian adjoint of itself ;

$$I = \vec{E}^\dagger \vec{E} \quad (2.51)$$

$$I = \begin{bmatrix} E_x^* & E_y^* \end{bmatrix} \begin{bmatrix} E_x \\ E_y \end{bmatrix} = E_x^* E_x + E_y^* E_y$$

Absolute intensity of the electric vector does not concern us at this moment, we can use unit intensity wave, which fulfills the requirement;

$$\vec{E}^\dagger \vec{E} = 1 \quad (2.52)$$

Specifically, in the case of linear polarization in the x-y plane (Figure 2.6), from eqs. (2.50) and (2.52), normalized electric vector is written as,

$$\vec{E} = \begin{bmatrix} \cos \beta \\ \sin \beta \end{bmatrix} \quad (2.53)$$

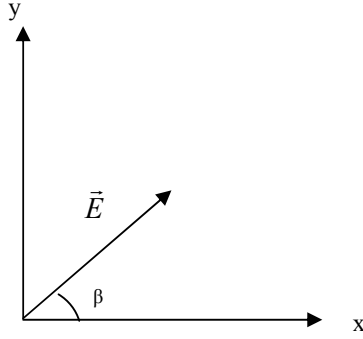


Figure 2.6 Oscillation direction of a wave in case of linear polarization.

2.7.3 Jones Matrices

Transmission Matrix: A transmission matrix of an isotropic material, which has a thickness d and refractive index n , simply adds a phase factor of e^{-iknd} to the field components, when multiplied with eq. (2.50). In matrix form the transmission matrix is

$$T = \begin{bmatrix} e^{-iknd} & 0 \\ 0 & e^{-iknd} \end{bmatrix} \quad (2.53)$$

where κ is the propagation coefficient in free space.

Reflection Matrix: On the contrary to transmission, in reflection, a sudden change occurs when the light beam is bounced off from the surface. If the surface has a reflection coefficients r_p and r_s , the reflection matrix is defined as

$$R = \begin{bmatrix} r_p & 0 \\ 0 & r_s \end{bmatrix} \quad (2.54)$$

Rotation Matrix (Transformation matrix): In case of a coordinate translation, Jones vectors have to be transformed also according to the transformation matrix. When the axis is rotated by α in counterclockwise direction, new coordinates is obtained by multiplying the old one with the transformation matrix shown below.

$$R(\alpha) = \begin{bmatrix} \cos(\alpha) & \sin(\alpha) \\ -\sin(\alpha) & \cos(\alpha) \end{bmatrix} \quad (2.55)$$

The overall effect of the optical system on the incident wave is obtained by multiplying all the matrices in the system in the order that light passes through and thus finding an overall matrix. Then eq.(2.56) can be used to calculate the output wave. According to these, if the input of the system is an electrical field with components E_{pi} and E_{si} , and the output is E_{po} and E_{so} , the relation between them is

$$\begin{bmatrix} E_{po} \\ E_{so} \end{bmatrix} = \begin{bmatrix} m_{11} & m_{12} \\ m_{21} & m_{22} \end{bmatrix} \begin{bmatrix} E_{pi} \\ E_{si} \end{bmatrix} \quad (2.56)$$

The first matrix on the right hand side is the overall system matrix.

2.8 Ellipsometry

2.8.1 Introduction

Ellipsometry is a technique that uses the state of polarization of light to derive information about the material from which the light is reflected (see also Chapter-3). It is generally very sensitive to surface roughness and cleanliness. Ellipsometry only gives two parameters, ψ and Δ , which are defined mathematically later in the chapter. Then using related equations, one can determine the film parameters such as, n , k and d . Multiple angle ellipsometry (MAI) in

which the angle of incidence of the beam can be changed, is usually used to measure the very thin (100 Angströms) oxide layer on a silicon substrate [7]. Also spectroscopic ellipsometry in which the wavelength of the light can be changed, is used dominantly for measurements.

2.8.2 Ellipsometry Equations

A Jones vector can be constructed that describes an elliptical vibration whose amplitude A , phase δ , azimuth angle θ and ellipticity angle ε [8]. (In Figure 2.5, these values are shown. In addition to that, phase angle δ is the angle of electric vector with the x-axis when $t = 0$).

$$\begin{bmatrix} E_x \\ E_y \end{bmatrix} = A e^{i\delta} \begin{bmatrix} (\cos \theta \cos \varepsilon - i \sin \theta \sin \varepsilon) \\ (\cos \theta \cos \varepsilon + i \sin \theta \sin \varepsilon) \end{bmatrix} \quad (2.57)$$

Although the Jones vectors provides a concise representation of the electric vibration of a wave, there are occasions where a simpler representation is more adequate. This is the case when the amplitude and absolute-phase information about the elliptic vibration of the electric vector are of secondary interest, justifying the suppression of such information. Azimuth and ellipticity angle information can be extracted from the eq. (2.50). If the ratio of its phasor components is taken, a new parameter χ is defined.

$$\chi = \frac{E_y}{E_x} = \frac{|E_y|}{|E_x|} e^{i(\delta_y - \delta_x)} \quad (2.58)$$

Using eq. (2.57), χ is found to be a complex function of the azimuth angle and the ellipticity angle.

$$\chi = \frac{\tan \theta + i \tan \varepsilon}{1 - i \tan \theta \tan \varepsilon} \quad (2.59)$$

Equation (2.59) shows explicitly how each elliptic state of polarization of given azimuth and ellipticity angle is represented by a single complex number χ . With each complex number χ , we can associate a representative point in the complex plane which thus provides a space in which to represent the states of polarization of light. This representation is called the cartesian complex plane representation. Now, consider any optical system that may change the polarization state of light. And the input of the system is the polarization state χ_i and output polarization state χ_o . The ratio of these values is,

$$\rho = \frac{\chi_i}{\chi_o} \quad (2.60)$$

$$\rho = \frac{E_{y,i}}{E_{x,i}} \frac{E_{x,o}}{E_{y,o}} = \frac{E_{y,i}}{E_{y,o}} \frac{E_{x,o}}{E_{x,i}} = \frac{r_x}{r_y} \quad (2.61)$$

Eq. (2.61) is a direct consequence of eqs. (2.58) and (2.19) when it is taken that $x \rightarrow p$, and $y \rightarrow s$, where the p and s are defined previously at section 2.3.

$$\rho = \frac{r_p}{r_s} \quad (2.62)$$

$$\rho = \frac{r_p}{r_s} = \left| \frac{r_p}{r_s} \right| e^{i(\Delta_p - \Delta_s)} \quad (2.63)$$

where $r_p = |r_p| e^{i\Delta_p}$ and $r_s = |r_s| e^{i\Delta_s}$ ρ is the fundamental parameter of ellipsometry.

It can be reduced to two parameters as,

$$\rho = \tan \psi e^{i\Delta} \quad (2.64)$$

where, $\tan \psi = \left| \frac{r_p}{r_s} \right|$ and $\Delta = \Delta_p - \Delta_s$

ψ and Δ are called ellipsometric angles. ψ is the angle whose tangent gives the ratio of the amplitude attenuation or magnification upon reflection for the p and s polarizations, and Δ gives the difference between the phase shifts experienced upon reflection by the p and s polarizations. In order to use the ellipsometry equations, the medium or system must be well-defined, from which the light is reflected. Some models are examined in the following sections.

2.9 Film-Substrate Systems

2.9.1 The Single Substrate

If there is only substrate as medium, then eq. (2.64) becomes,

$$\rho = \frac{N_s \cos \theta_0 - n_0 \cos \theta_s}{N_s \cos \theta_0 + n_0 \cos \theta_s} \times \frac{n_0 \cos \theta_0 + N_s \cos \theta_s}{n_0 \cos \theta_0 - N_s \cos \theta_s} \quad (2.65)$$

N_s is the complex index of refraction of the substrate, n_0 is the real index of the outer medium. Generally this medium is air and the index is taken as one. From the above equation, the real (n_s) and imaginary (k_s) parts of the N_s can be calculated,

$$N_s = n_0 \tan \theta_0 \sqrt{1 - \frac{4\rho}{(1+\rho)^2} \sin^2 \theta_0} \quad (2.66)$$

or,

$$n_s^2 - k_s^2 = n_0^2 \sin^2 \theta_0 \left(1 + \frac{\tan^2 \theta_0 (\cos^2 2\psi - \sin^2 \Delta \sin^2 2\psi)}{(1 + \sin 2\psi \cos \Delta)^2} \right) \quad (2.67)$$

$$2n_s k_s = \frac{n_0^2 \sin^2 \theta_0 \tan^2 \theta_0 \sin 4\psi \sin \Delta}{(1 + \sin 2\psi \cos \Delta)^2} \quad (2.68)$$

2.9.2 Air-film-Substrate System

An important phenomena in ellipsometry occurs, when polarized light is reflected from a film of thickness d on a substrate with the angle of incidence θ . It is assumed that, the planes are parallel and smooth. From eq. (2.25) and eq. (2.64),

$$\rho = \frac{r_{01p} + r_{12p} e^{-2i\beta}}{1 + r_{01p} r_{12p} e^{-2i\beta}} \times \frac{1 + r_{01s} r_{12s} e^{-2i\beta}}{r_{01s} + r_{12s} e^{-2i\beta}} \quad (2.69)$$

ρ is a function of n_s, n, k, d, θ and λ for an air-film-substrate system. Generally n, k and d are the unknowns of film. Theoretically, in multiple angle ellipsometry angle of incidence can be changed, therefore from three equations with three unknowns, n, k and d can be determined. Two measurements give four equations, because of the real and imaginary parts in eq. (2.69). But practically these equations are transcendental and numerical techniques must be used.

In general the oxide layer, which is grown on the film and the surface micro roughness, where the mean height of the irregularities are less than the wavelength of light may affect the ellipsometer measurements. Therefore we can consider these two effects as different layers. The oxide layer is simple to model. It has a refractive index of 1.47.

In order to model the surface micro roughness, the combination of the material and the voids can be considered to make up an “effective layer”. To calculate the index of the effective layer, effective medium approximations (EMA), such as Lorenz-Lorenz, Maxwell-Garnett, and Bruggeman EMA, can be used. In

Bruggeman EMA, the dielectric function of the effective layer obeys the equation below [9].

$$(1 - c) \frac{\varepsilon_1 - \varepsilon}{\varepsilon_1 + 2\varepsilon} = c \frac{\varepsilon - \varepsilon_2}{\varepsilon_2 + 2\varepsilon} \quad (2.70)$$

Where c is the concentration of the inhomogeneity with dielectric constant ε_2 , considered on the layer. ε_1 is the dielectric constant of the material, and finally ε is the dielectric constant of the effective medium. In order to define a layer, the index and thickness values of the effective medium is put in a matrix explained later in section 2.10.

Now that there are multiple surfaces on the substrate, simple methods become more complex to determine reflection coefficients to find ρ . Therefore another method is needed to handle multiple films on a substrate. Section 2.10 introduces a method for multiple films.

2.9.3 Dependence of ρ on the Film Thickness

The dependence of ρ on the film thickness is important in ellipsometry. Because more than one thickness value fit the ellipsometric equations. Eq. (2.69) can be cast in the form [8],

$$\rho = \frac{A + BX + CX^2}{D + EX + FX^2} \quad (2.71)$$

Where $X = e^{-i2\beta}$, $A = r_{01p}$, $B = r_{12p} + r_{01p}r_{01s}r_{12s}$, $C = r_{12p}r_{01s}r_{12s}$ $D = r_{01s}$,

$E = r_{12s} + r_{01p}r_{12p}r_{01s}$, $F = r_{01p}r_{12p}r_{12s}$.

X can also be written by using the relation ($\beta = 2\pi\left(\frac{d}{\lambda}\right)\cos\theta_1$) and snell's law as;

$$X = \exp[-i2\pi(d / D)] \quad (2.72)$$

where

$$D = \frac{1}{2} \lambda (N_1^2 - N_0^2 \sin^2 \theta_0)^{-1/2} \quad (2.73)$$

ρ is a function of X , and according to eq. (2.72), X is a periodic function of d (thickness of the film) so infinite values of d may give the same X . Therefore, in order to use the ellipsometry equations, a rough estimate of the film thickness is needed.

2.10 Multilayer Films

The reflection and transmission coefficients of a single film on a substrate are found by using eqs. (2.25) and (2.26), but when multilayer films are involved some new methods should be used. Treatment for such a generalized situation can be found in [3, 6].

If an EM wave of magnitude E_0 and a wave vector $\vec{\kappa}$ strikes on top of a medium of multilayer films, infinite number of oscillations are created inside the slab of films, caused by multiple reflections and transmissions from surfaces. Each layer can be denoted by the characteristic matrix of the medium.

Consider a medium of thickness d , sandwiched between any two surfaces, for example surface (a) and surface (b). In addition, suppose E_a and B_a are the electric and magnetic fields at the surface (a), E_b and B_b are the electric and magnetic fields at the surface (b). The relationship between them is found by using boundary conditions as [3]

$$\begin{bmatrix} E_a \\ B_a \end{bmatrix} = \begin{bmatrix} \cos \delta & i \sin \delta / \gamma_n \\ i \gamma_n \sin \delta & \cos \delta \end{bmatrix} \begin{bmatrix} E_b \\ B_b \end{bmatrix} \quad (2.74)$$

For the n^{th} medium. In this equation $\delta = \left(\frac{2\pi}{\lambda}\right)nd \cos \theta$, $\gamma_n = n_n \sqrt{\epsilon_0 \mu_0} \cos \theta_n$ for

TE and $\gamma_n = \frac{n_n \sqrt{\epsilon_0 \mu_0}}{\cos \theta_n}$ for TM. The reflection and transmission coefficients for the

medium are

$$r = \frac{(m_{11} + m_{12} p_l) p_1 - (m_{21} + m_{22} p_l)}{(m_{11} + m_{12} p_l) p_1 + (m_{21} + m_{22} p_l)} \quad (2.75)$$

$$t = \frac{2 p_1}{(m_{11} + m_{12} p_l) p_1 + (m_{21} + m_{22} p_l)} \quad (2.76)$$

m_{ij} represents the matrix components in eq. (2.74). For multiple films, overall characteristic matrix is the multiplication of the individual characteristic matrices of the media, in the order that light encounters. This process will be used when making a numerical simulation of thin films on a substrate (Del, Psi vs Ang. of inc. curves).

2.11 Conclusion

In this chapter starting from the well-known Maxwell equations, Fresnel coefficients, that relating the incident amplitude on a optical system to transmitted and reflected ones, are introduced. Some techniques used in the experiments are explained. Each elliptical polarization state can be represented by a parameter defined as χ . This definition leads to classical ellipsometry equations which allows user to know the sample properties using the ellipsometer itself.

CHAPTER 3

INSTRUMENTATION

3.1 Plasma System (Plasma Enhanced Chemical Vapor Deposition)

3.1.1 Overview

In thin film technology Chemical Vapour Deposition (CVD) technique which creates thin films of material on a substrate via the use of chemical reactions, is mostly used. Reactive gases are fed into a vacuum chamber and these gases react on a substrate and form a thin film. In Plasma Enhanced Chemical Vapour Deposition (PECVD) technique, the reactive gases are caused to decompose via the electrical discharge. This causes films to deposit at lower temperatures than CVD as an advantage. Let us outline the PECVD system for seizing the eventual roles of various plasma parameters during film deposition.

The growing field of applications of plasma as deposition, etching, surface modification and chemical conversion has stimulated a renewed interest in plasma science in the atomic physical chemistry regime. Plasma media are generated by supplying energy to neutral gas molecules causing the formation of charge carriers and radicals [10]. In other words, electrons and ions are produced in the gas phase when electrons or photons with sufficient energy collide with the neutral atoms and molecules in the feed gas.

The most commonly used method of generating and sustaining a low-temperature plasma is by applying an electric field to a neutral gas medium across

two facing parallel electrodes (Figure 3.1). Any volume of a neutral gas always contains a few electrons and ions that are formed, for example, as a result of the interaction of cosmic rays or radioactive radiation with the gas. These free charge carriers are accelerated by the existing electric field and new charged particles may be created when these charge carriers collide with atoms and molecules in the medium. This leads to an avalanche of charged particles that is eventually balanced by charge carrier losses which occur due to various reasons such as drift and diffusion to the reactor walls (boundaries), recombination (ion-ion recombination, electron-ion recombination) and attachment to electronegative molecules so that a steady-state plasma develops (plasma is self-sustained). As a result, the gas medium between electrodes starts to conduct electrical current. In practice ac and dc voltages are both applied. But RF (Radio frequency) discharges are especially useful when the layer to be treated is a semiconductor or an isolator [11]. Since a dc discharge current can not be sustained, alternating current is required. The frequency of this alternating voltage must be so high that the charged particles created in one half of the RF cycle are not lost when the current goes through zero. The frequency range thus needed is typically between 50 kHz-15 MHz. There are three types of event in the plasma [12]:

1. Elastic collisions: Momentum and energy are both conserved.
2. Inelastic collisions: Momentum is conserved. But a fraction of the initial kinetic energy is transferred to internal energy in one or more of the particles (i.e. excited states or ions are formed)
3. Superelastic collisions: there is more kinetic energy after the collision. Momentum is conserved and internal energy in the particles entering into a collision is transferred into kinetic energy.

A schematic diagram of capacitively coupled radio frequency discharge is given in Figure 3.1 [13]. For a gas pressure of about 1 torr, a weakly ionized medium (10^{10} electrons or ions per cm^3 , 10^{16} neutral molecules per cm^3) is obtained between

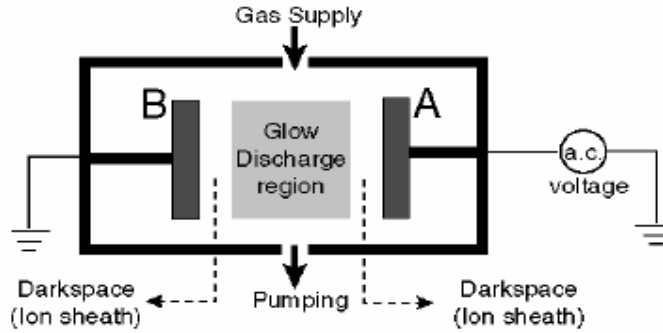


Figure 3.1 Capacitively coupled radio frequency discharge.

the electrodes. In the dark regions near the electrodes, electrons cause ionization and lose energy upon entering the glow discharge region and cause only excitation, these excited atoms or molecules while returning to ground states, emit radiation and the region seems glowing.

3.1.2 Interaction of the Plasma with Substrate

Following sequence of phenomena are observed in the interaction of the plasma with the substrate [14].

1. bulk transport of reactants into the process volume
2. gaseous diffusion of reactants to the surface
3. adsorption of reactants onto the surface
4. surface reaction
5. surface diffusion
6. lattice incorporation
7. reaction by-product desorption
8. gaseous transport of by-products
9. bulk transport of by-products out of process volume.

The diagram of the PECVD reactor which is used in the deposition of the films is given in Figure 3.2. Gas cabinet system of the PECVD reactor is shown in Figure 3.3.

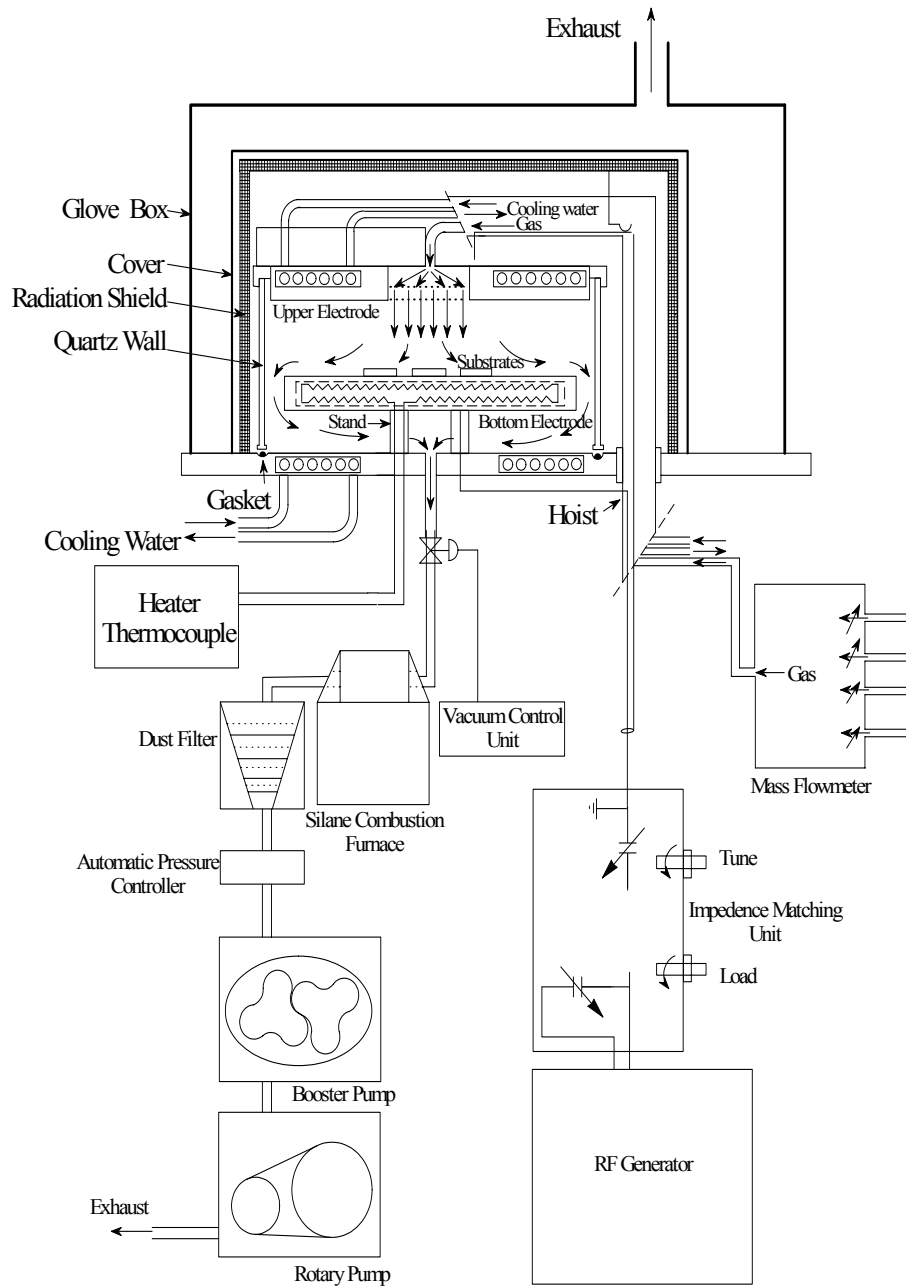


Figure 3.2 PECVD system which is used in the production of thin films [15].

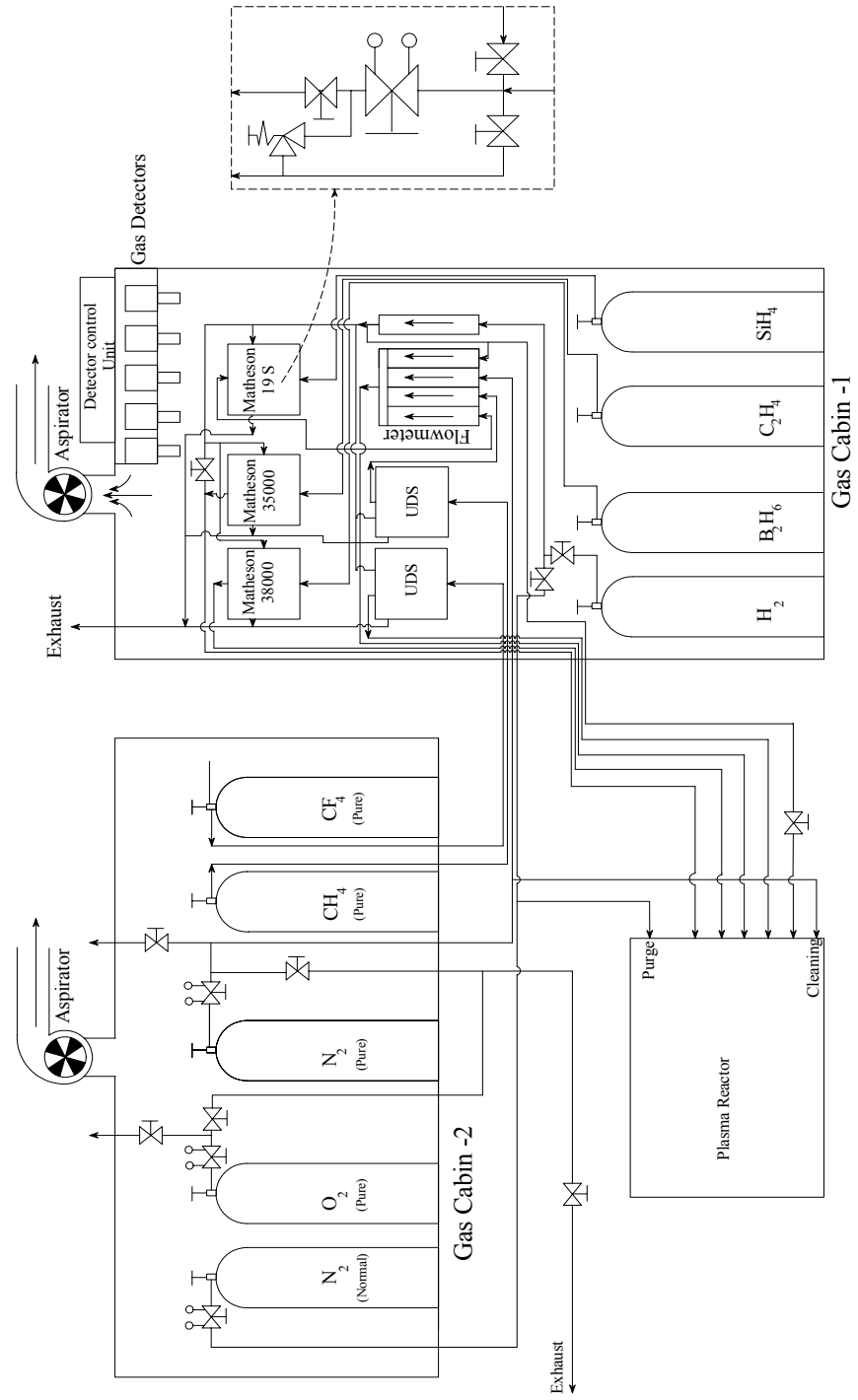


Figure 3.3 Gas cabinet system in the PECVD mechanism [15].

3.2 UV-Visible Spectrometer (Perkin Elmer Lambda 2S)

Spectrometer is used as a part of the optical measurement process. Physically, the device sends a light beam of wavelength between 200-1100 nm. at zero angle of incidence to the sample. Transmittance spectrum is like in Figure 2.4. That allows calculations related to the optical properties of the sample. The Principles of operation of the spectrometer used is as follows.

The optical path of the Lambda 2 is represented in Figure 3.4 on the following page [16]. The monochromator is a concave holographic grating with 1053 lines/mm. Planar mirror P1 is moved into position by a mechanical arm. When it is in position, light from the deuterium lamp DL (ultraviolet radiation), is blocked, and light from the halogen lamp HL (visible radiation), is reflected onto the toroidal mirror T2. Source changes, due to the positioning of mirror P1, occur in synchronization with the monochromator, at a specified wavelength. The monochromator stops slewing until the source change is complete.

Radiation is focused by T2, passing through the filter Wheel (FW) onto the entry slit ES1. The filter Wheel rotates different optical filters into the radiation beam. It is synchronized with the monochromator. The filters serve to limit the wavelength range reaching the monochromator, and so reduce stray radiation. Radiation passes through the entry slit to the monochromator. Radiation is spectrally dispersed by the monochromator and focussed on the exit slit ES2.

After passing through the exit slit, radiation passes to the spherical mirror s3. Radiation is reflected onto the beam splitter BS, which allows 50% of the radiation to pass through to planar mirror p4. 50% of the radiation is reflected onto planar mirror p5. Mirror p4 focusses the radiation beam in the sample cuvette. The radiation is then focused onto the sample photo-diode detector by a simple convex lens. Mirror p5 focuses the radiation beam in the reference cuvette. The radiation is then focused onto the reference photo-diode detector by a simple convex lens.

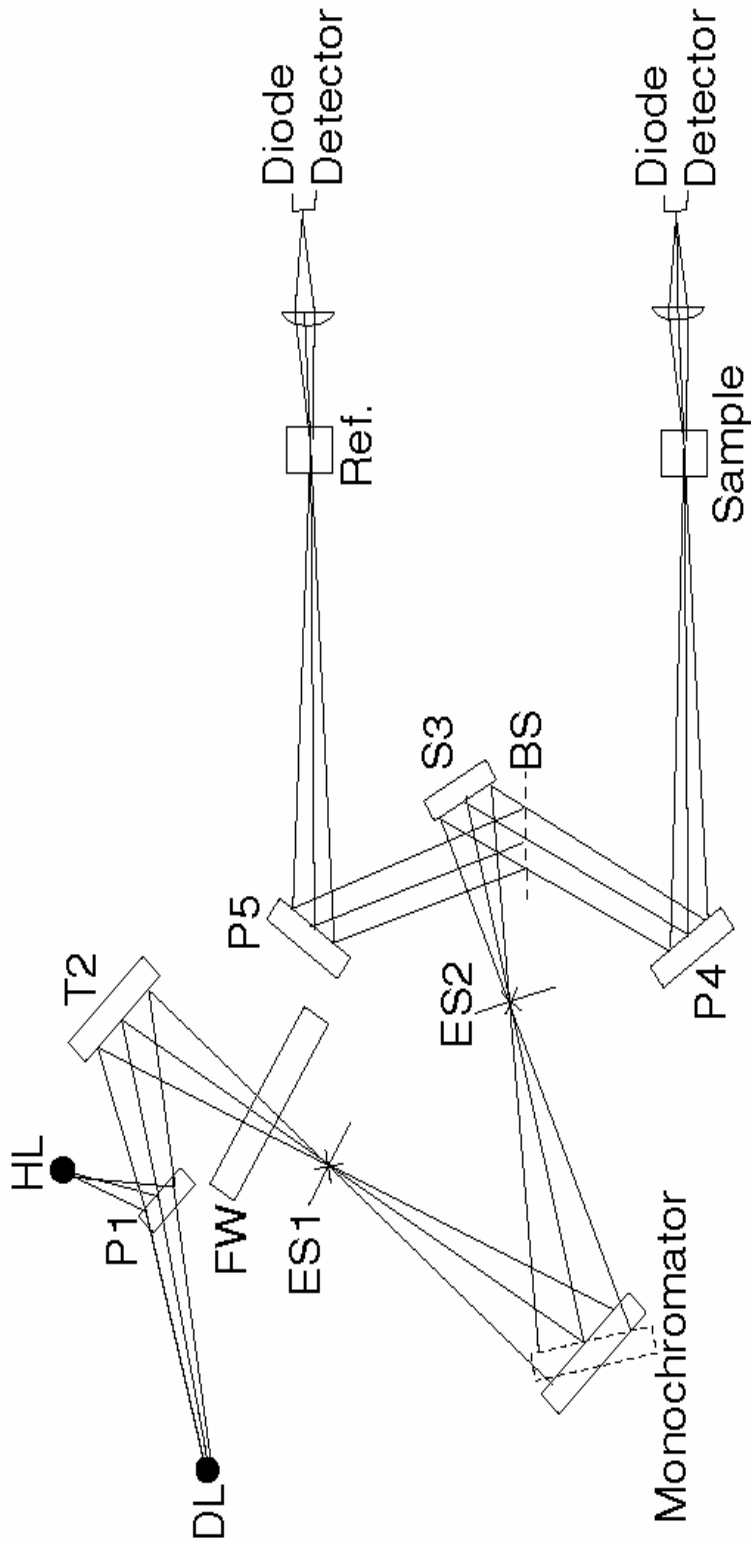


Figure 3.4 Diagram of the optical path of the Perkin-Elmer Lambda 2 Spectrometer

3.3 The Ellipsometry Setup

In this part, first of all the optical components used in the devices are discussed briefly. The functions of the devices are emphasized rather than the inner physical mechanisms in the optical components [17].

3.3.1 Optical Elements

Polarizers: The polarizer is an optical element which has transmission and extinction axes. If the transmission axis of the polarizer lines up with the angle of polarization of the wave, the entire wave is transmitted. But, when the axis does not line up with the angle of polarization of the wave, the component along the transmission axis can pass whereas the other disappears. If the axis of the polarizer is perpendicular to the angle of polarization no light is transmitted and a 'null' is obtained. The polarizer is used to convert unpolarized light into polarized light.

Analyzers: If a polarizer is used to determine the state of polarized light by locating the null, it is called analyzer.

Quarter wave plates (QWP): These are anisotropic optical elements. In QWP the velocity of the wave depends on its orientation, therefore an extra phase difference is added between the components of the wave.

3.3.2 The Ellipsometer

Ellipsometers are opto-electronic measuring instruments of very high precision, which are mainly used to determine optical characteristics of materials and to measure the thickness of very thin films on surfaces. The principle of ellipsometry is based on the physical effect that the polarized light, which is reflected from a surface, changes its state of polarization (Figure 3.5). In null

ellipsometry [18], there is a quarter-wave plate between the polarizer and the system or between the analyzer and the system and in principle, it is based on determining a set of angles for the polarizer, compensator (quarter wave plate) and the analyzer such that the light flux falling on the photodetector is extinguished (null). On the other hand in photometric ellipsometry, the principle is based on utilization of the variation of the detected light flux as a function of some parameters. In summary, The device determines ψ and Δ by means of (eq. (3.3)) after interaction of the light with the material under investigation. Then material properties may be found by using related fresnel coefficients and suitable physical model. Ellipsometry is much more sensitive than other measuring methods in this field. Even the thickness of an atomic layer can be measured. Multi-layer thin films can be determined by several measurements again using a suitable model. In contrast to some other measuring methods (e.g. Electron microscopy or chemical methods), the ellipsometry is a non-destructive method. It requires no vacuum and generally no special preparation of the sample.

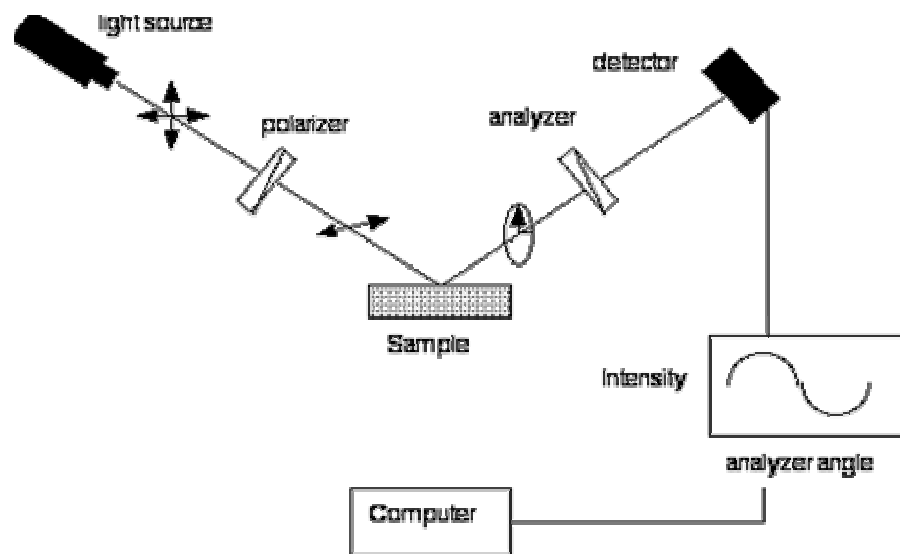


Figure 3.5 Optical setup of photometric Ellipsometry

Figure 3.6 shows the optical path of the rotating analyzer ellipsometer. p and s axes refer to the coordinates of the electric field coming out of the laser source (L), t and e axes refer to the transmission and extinction axes of the polarizers.

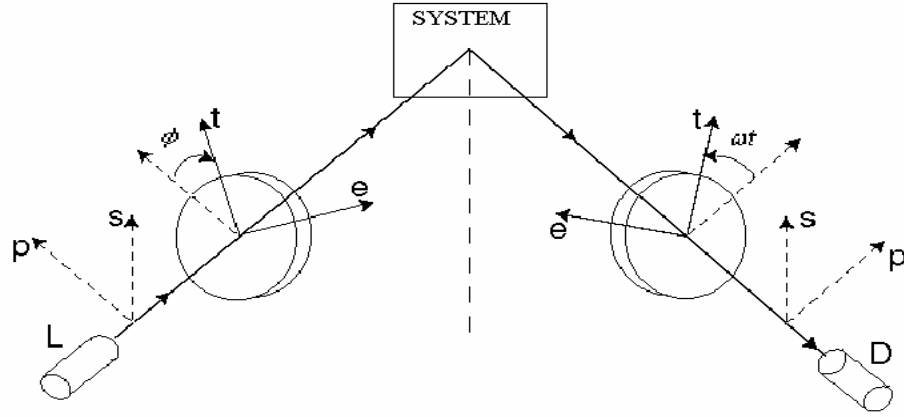


Figure 3.6 Principles of ellipsometric measurement

Using Jones matrices from chapter 2, the equation for Figure 3.6. can be written as in eq. (3.1). An unpolarized light beam first passes through the polarizer. The first matrix on the right hand side is the polarization state of light after passing through the polarizer with the polarizer angle ϕ (eq. (2.53)). Then it is reflected back from the optical system and comes to the analyzer that is rotating with angular velocity ω . The axes of the light should be changed to the analyzer axes by using rotation matrix. And the leftmost matrix on the right hand side is written for analyzer by putting zero in place of extinction coefficient and only one axis is assumed for transmission in eq. (2.53). Finally, according to the above discussion, it can be written that,

$$\vec{E} = E_0 \begin{bmatrix} 1 & 0 \\ 0 & 0 \end{bmatrix} \begin{bmatrix} \cos \omega t & \sin \omega t \\ -\sin \omega t & \cos \omega t \end{bmatrix} \begin{bmatrix} r_p & 0 \\ 0 & r_s \end{bmatrix} \begin{bmatrix} \cos \phi \\ \sin \phi \end{bmatrix} \quad (3.1)$$

E_0 is the amplitude of the electric vector.

$$\vec{E} = E_0 \begin{bmatrix} r_p \cos \phi \cos \omega t + r_s \sin \phi \sin \omega t \\ 0 \end{bmatrix}$$

$$I = E_0^2 |r_p \cos \phi \cos \omega t + r_s \sin \phi \sin \omega t|^2 = E_0^2 r_s^2 \left| \frac{r_p}{r_s} \cot \phi \cos \omega t + \sin \omega t \right|^2 \quad (3.2)$$

$$= E_0^2 r_s^2 |e^{i\Delta} \tan \psi \cot \phi \cos \omega t + \sin \omega t|^2$$

$$I = I_0 (\alpha \cos 2\omega t + \beta \sin 2\omega t + 1) \quad (3.3)$$

where,

$$I_0 = E_0^2 r_s^2 \cot^2 \phi \frac{\tan^2 \psi + \tan^2 \phi}{2}, \quad \alpha = \frac{\tan^2 \psi - \tan^2 \phi}{\tan^2 \psi + \tan^2 \phi}, \quad \beta = \frac{2 \tan \phi \cos \Delta \tan \psi}{\tan^2 \psi + \tan^2 \phi}$$

Particularly, its used mostly in literature to be $\phi = 45^\circ$, then we have,

$$I_0 = \frac{E_0^2 r_s^2}{2 \cos^2 \phi}, \quad \alpha = -\cos 2\psi \quad \text{and} \quad \beta = \sin 2\psi \cos \Delta \quad (3.4)$$

From these equations ψ and Δ can be calculated.

3.3.3 Specifications of the Ellipsometer At Hand

In measurements, EL X-02C ellipsometer is used (Figure 3.7). Specifications of the device are as follows [19]:

- The EL X-02C high precision ellipsometer contains ellipsometer mechanics and software to use it via a computer.
- The ellipsometer mechanics consist of a transmitter unit and a receiver unit fixed at the end of adjustable arm.

- The transmitter unit consists of a helium-neon laser of 632.8 nm wavelength.
- A polarizer is available inside the transmitter.
- The receiver unit consists of a polarizing prism as analyzer, which is connected to a stepper motor.
- The receiver unit also contains four detectors consisting of photodiode arrays.
- The angle of incidence is adjustable in steps of 5 degrees by pin location. The range is 90 to 30 degrees.
- The EL X-02C high precision ellipsometer is able to measure thin films between 0.1 and 600 nm with an accuracy of 0.1 nm.

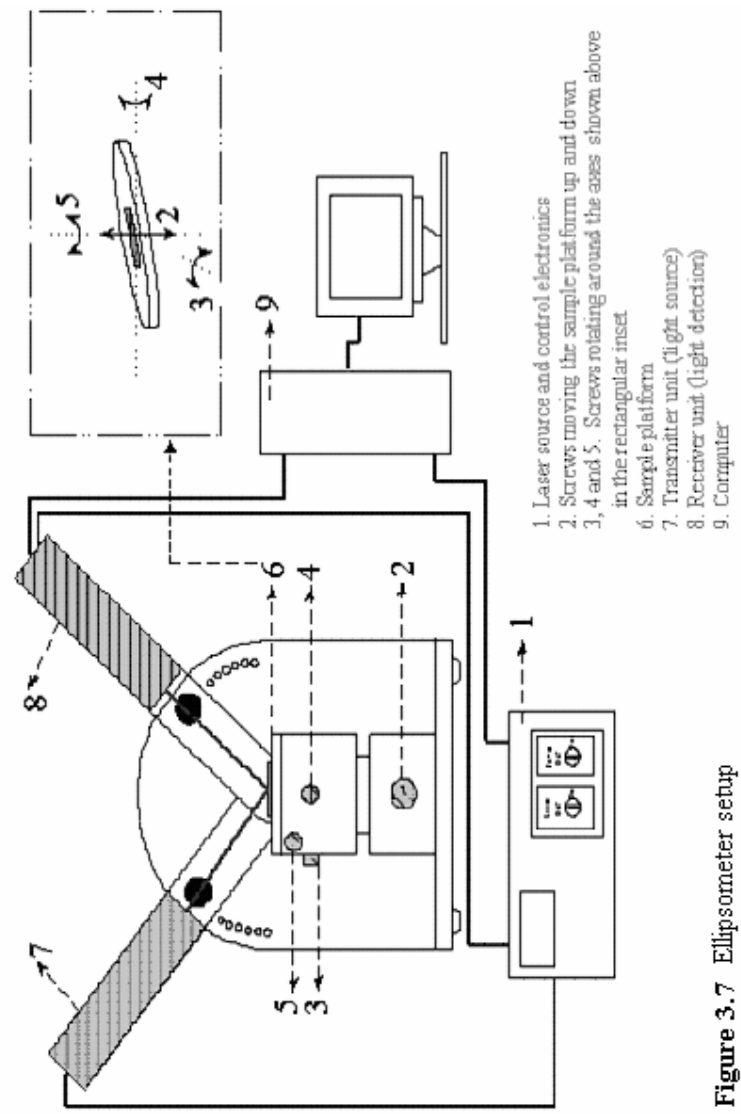


Figure 3.7 Ellipsometer setup

3.3.4 Operating Principles

Before making measurements on the device some adjustments have to be made.

These can be summarized as follows:

1. Intensity Test Step: The arms of the ellipsometer are brought into horizontal position (Figure 3.8). The device controls whether the light can reach the detectors with enough intensity.
2. Rest intensity Measurement Step: The rest light intensity of the medium is measured and stored. In general, the lesser the light intensity of the medium, the more accuracy of the measurement.
3. Calibration step : In this step, polarization of the laser light is determined without any reflection from a surface.

After preparation of the device, the sample is put on the sample platform. Angle of incidence is adjusted by moving the arms. Before the measurement is made, one more condition have to be fulfilled.

4. Sample Alignment Step: At last, before the measurement is made, the sample have to be aligned using screw mechanics in Figure 3.7., so that four detectors in the receiver unit get enough intensity.

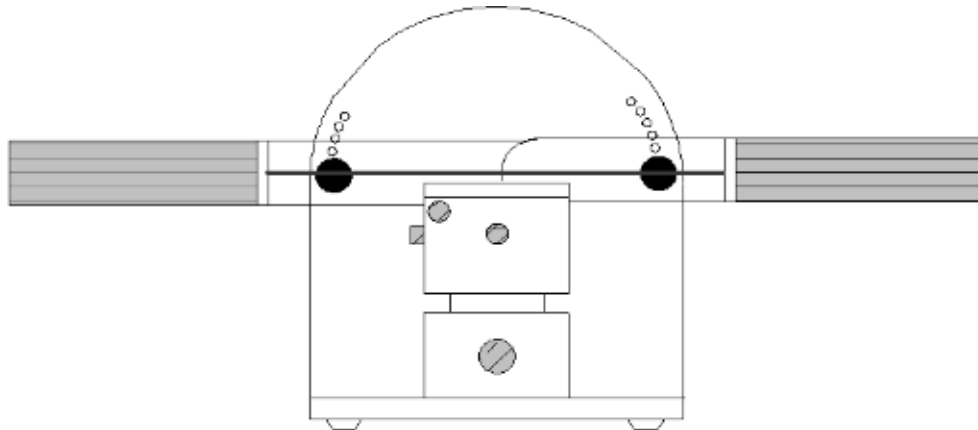


Figure 3.8 Ellipsometer before measurement. For calibration purposes, transmitter and receiver units have to be aligned before measurement.

CHAPTER 4

EXPERIMENTAL STUDIES

4.1 Optical Absorption in Solids

In the case of an interaction between the light and crystal, a small term is added to the Hamiltonian of the electron. This time-dependent perturbation which is caused by electron-photon interaction leads to electronic transitions from state to state. In order to find the probability of this transition, a new wave function, constructed from the superposition of the wavefunctions before the illumination, is considered. By solving the Schrodinger equation, the transition probability can be found. The probability is seen to be non-zero when the photon energy is beyond the gap energy E_g . It is well known that in a crystalline structure, the crystal momentum or wavevector (κ), deduced from the structural periodicity, is the “quantum” number defining the state of the electron through the so-called Bloch function. Energy and wave vector are conserved as a result of this optical transition.

Transition probability is related to absorption coefficient such that the probability of transition per unit time over photon flux is equal to absorption cross section, which is essentially absorption coefficient per absorbing atomic center. In order to find the energy gap, absorption coefficient may be dragged from above definition and integrated over the crystal. If the band gap of the material is a direct band gap, the maximum of the valence band and the minimum of the conduction band coincide in the momentum space and momentum conservation is satisfied without the requirement of phonon contribution. On one side, considering this

crystal momentum (or κ vector) conservation, on the other side taking into account the square root energy dependence of the densities of states around the both valence and conduction band edges, $g_v(E) = A(E_v - E)^{1/2}$ and $g_c(E) = B(E - E_c)^{1/2}$ respectively, where A and B are constants, the dispersion relation of the absorption coefficient α as a function of the photon energy $\hbar\omega$ may be found as:

$$\alpha = \frac{\beta_c (\hbar\omega - E_g)^{1/2}}{\hbar\omega} \quad (4.1)$$

Where β_c is constant. E_g may be obtained from the experimental dispersion relation of the absorption coefficient (α vs. $\hbar\omega$) by plotting $[\hbar\omega\alpha(\hbar\omega)]^2$ vs. $\hbar\omega$ and extrapolating to the horizontal energy axis.

In a crystalline semiconductor, the conduction and valence band distributions of states terminate abruptly at their respective band edges and forbidden energy gap occurs. In contrast, in an amorphous semiconductor, the distributions of conduction band and valence band states do not terminate abruptly at the band edges [20]. Instead, some extended states encroach more or less deep into the gap region, the distribution of these localized tail states arising as a consequence of the both bond length and bond angle disorders decreases exponentially as a function of the energy depth from the relevant band edge (see Figure 4.1). In addition to tail states, there are also states deep within the gap region, due to structural defects, such as vacancies and dangling bonds, whose density is Gauss-like distributed (Figure 4.1). Thus, in an amorphous semiconductor, there is no true gap in the distribution of electronic states. Despite this fact, from the upper edge of valence extended states to the lower edge of conduction extended states a “pseudo” gap has been defined, called optical gap or mobility gap.

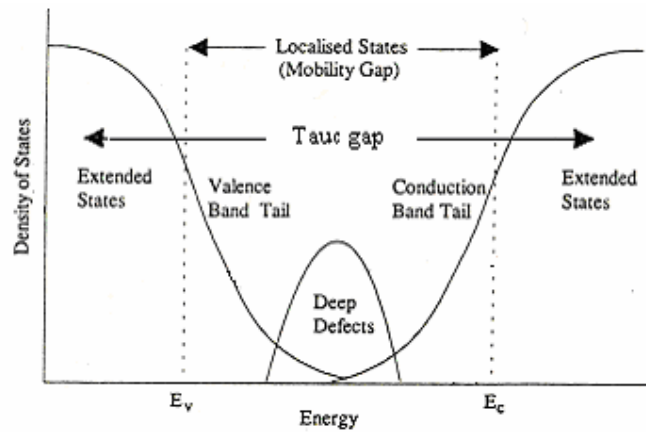


Figure 4.1 Schematic diagram of the density of states in amorphous semiconductors.

In defining the band structure of amorphous materials, measures of the gap which is related to measurements of the optical absorption spectrum, $\alpha(\hbar\omega)$, referred to as measures of the optical gap, are the most common. Unfortunately, there is no pronounced feature of the optical absorption spectrum of an amorphous semiconductor which can be directly related to an optical gap. While the optical absorption spectrum associated with a crystalline semiconductor terminates abruptly at the fundamental gap. A tail in the optical absorption spectrum, arising as a consequence of the tail and gap states, makes the optical gap of an amorphous semiconductor difficult to define experimentally.

In order to derive an expression for the energy gap value in amorphous semiconductors, it must be considered that crystal momentum or k vector is not well-defined in amorphous solids on the contrary to crystalline one. In other words, This is caused by the vanishing periodicity leading to the confinement of the electron within a region of finite extent as a result according to Heisenberg's principle the momentum information loses its certainty. And momentum conservation is no longer used. There are 5 types of optical transitions in amorphous semiconductors:

- (a) transitions between valence and conduction band extended states,
- (b) transitions between valence band tail and conduction band extended states,
- (c) transitions between valence band extended and conduction band tail states
- (d) transitions between valence and conduction band tail states.
- (e) transitions between mid-gap states (dangling bonds) and extended states.

In this work, only the optical transition between valence band extended states to conduction band extended states will be considered in order to obtain an analytical expression of the absorption coefficient α as a function of photon energy. In this respect, the κ vector conservation is assumed relaxed, in other words each k vector is only defined within an uncertainty of $\pm \Delta\kappa$. This practical removal of κ vector conservation may be interpreted as follows: a photon of energy $\hbar\omega$ is able to transfer an electron around edge of the valence band at energy E to a state of any κ -vector at the energy $E+\hbar\omega$. Finally, omitting the κ vector conservation, and assuming the same density of state distributions as in crystalline case (relation 4.1) around the mobility band edges, the dispersion relation of absorption coefficient may be obtained as [21]

$$\alpha = \frac{\beta_a(\hbar\omega - E_g)^2}{\hbar\omega} \quad (4.2)$$

Where β_a is a constant. The optical gap E_g may be found from the experimentally measured α vs. $\hbar\omega$ curve by plotting $\sqrt{\hbar\omega\alpha(\hbar\omega)}$ vs. $\hbar\omega$, and extrapolating the linear region to the energy axis. As discussed above, this expected linear region might be masked by other types of optical transitions and the determination of E_g may be erroneous or impossible. A practical solution to this difficulty has been produced by defining a formal energy gap E_{04} corresponding to the absorption coefficient of value 10^4 cm^{-1} .

4.2 Hydrogenated amorphous silicon carbide (a-Si_{1-x}C_x:H) Thin Films

The properties of the a-Si_{1-x}C_x:H are a mixture of both a-Si and a-C. The value of x determine the bonding organization changing from x = 0 (pure a-Si) to x = 1 (pure a-C). For x < 0.5, both Si-Si homonuclear bonds and Si-C heteronuclear bonds, for x ≈ 0.5 mainly Si-C heteronuclear bonds, and for x > 0.5 both Si-C and various types of homonuclear C-C bonds are expected.

The optoelectronic properties of the material is determined by its carbon concentration. And, it is important to understand the chemistry of a-Si_{1-x}C_x:H. For that reason, nature of the a-Si and a-C structures must also be known.

4.2.1 Structure of the a-Si

Silicon has four valence electrons. By sp³ hybridization, it forms four hybrid bonds with its neighbours (Figure 4.3). Basic shape is tetrahedral with an angle of 109.5°, between neighbours.

Si atom ground state								
1s ²	2s ²	2p _x ²	2p _y ²	2p _z ²	3s ²	3p _x ²	3p _y ²	3p _z ²
↑↓	↑↓	↑↓	↑↓	↑↓	↓↑	↓↑		

Figure 4.2 Electron configuration of Si atom in ground state.

Si atom sp ³ hybridization								
1s ²	2s ²	2p _x ²	2p _y ²	2p _z ²	3sp ³	3sp ³	3sp ³	3sp ³
↑↓	↑↓	↑↓	↑↓	↑↓	↓	↓	↓	↓

Figure 4.3 Electron configuration of Si atom in case of sp³ hybridization.

Opposite to the crystal structures where long range order dominates, in amorphous material only short range order exists. The disordered structure of the amorphous silicon affects the energy band structure, optical and electrical characteristics of the

material. The reason for the disorder is the bond strain within the amorphous structure. The strains lead to structural disorders, such as cracks or voids. As a result, coordination defects called dangling bonds (broken bonds) arise, reducing the overall strain by lowering average bond per atom. These defects prevent doping by capturing the dopant charge carriers. Therefore, in order to have an optoelectronic material, these dangling bonds must be reduced. Hydrogenation reduces the density of dangling bonds by saturating these bonds. It increases the band gap of the material because hydrogen is more electronegative than silicon. Further hydrogenation or limited dehydrogenation does not affect dangling bonds very much.

4.2.2 Structure of the a-C

The electrons of the carbon atoms form sp^3 , sp^2 and sp^1 types of hybridization in compounds. In a-C, generally sp^3 and sp^2 are seen in any ratio depending on the production conditions. Carbon atom has four valence electrons, the electron configuration in ground state can be written as,

C atom ground state				
$1s^2$	$2s^2$	$2p_x$	$2p_y$	$2p_z$
$\uparrow\downarrow$	$\uparrow\downarrow$	\downarrow	\downarrow	

Figure 4.4 Electron configuration of C atom.

When carbon atom makes a bond, hybridization may occur in which case two or more orbitals start to combine as one to provide stability and optimizing in energy. In sp^3 hybridization (Figure 4.5), each carbon atom forms tetrahedral structures with angles 109.5° with each other. Every atom has bonded to four neighboring atoms with four identical sp^3 bonds (σ). These bonds have characteristics of $1/4s$ and $3/4p$ type orbitals.

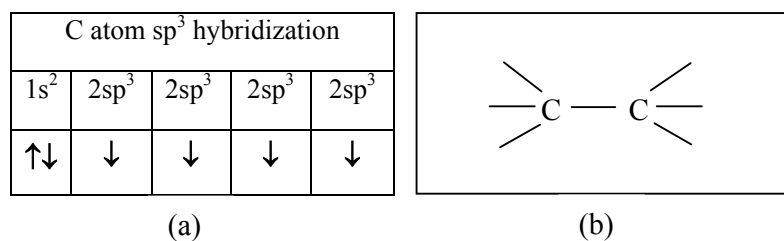


Figure 4.5 Carbon atom (a) Electron configuration in sp^3 hybridization, (b) bonding sketch where all the bonds are σ .

In sp^2 hybridization (Figure 4.6), three identical sp^2 orbitals and one unhybridized orbital in different peculiarity produce three σ bonds and one π bond respectively, which are very different from each other. Atoms tend to make bonds with three neighbouring atoms, forming a planar structure, where the atoms make 120° angles with each other. These bonds have a characteristics of $1/3$ s and $2/3$ p type orbitals.

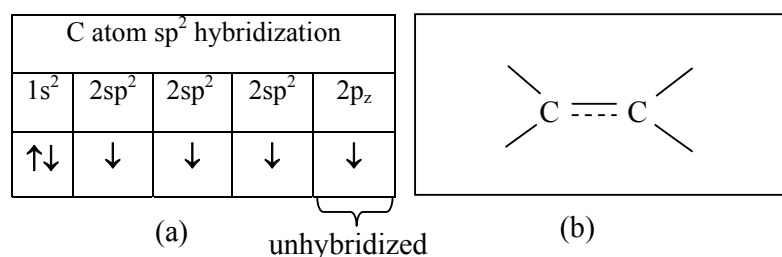


Figure 4.6 Carbon atom (a) Electron configuration in sp^2 hybridization, (b) bonding sketch where all the bonds are σ except for the dashed line which is actually a π bond.

Finally sp^1 type of hybridization includes participation of two hybridized and two unhybridized orbitals. Therefore two σ and two π bonds form in a linear structure. These bonds have a characteristics of $1/2$ s and $1/2$ p type orbitals.

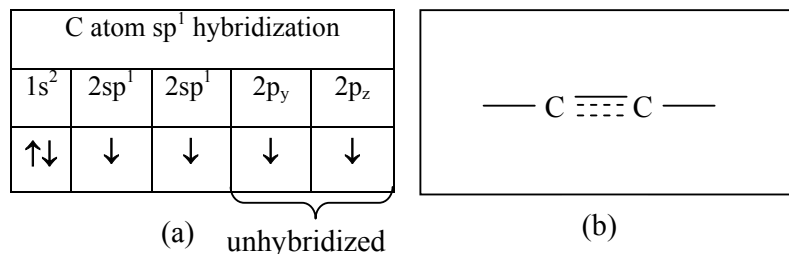


Figure 4.7 Carbon atom (a) Electron configuration in sp^1 hybridization, (b) bonding sketch where all the bonds are σ except for the dashed lines which are the π bonds.

4.2.3 Structure of the Bonds

The sp^3 hybridization forms four σ bonds where one s and one p orbitals participate, the result is tetrahedral structure with angles 109.5° (Figure 4.8(a)). Electrons forming the bonds are localized. In other words, electron can not easily escape from its location due to short coherence length of wave function. Therefore tetrahedral structure is an insulator or a semiconductor as in diamond. In sp^2 hybridization (Figure 4.8(b)), the first bond between carbon atoms is the σ bond in which one s and one p orbitals again participate and electrons are localized. The π orbitals, which are more complex, are formed after the σ . These π bonds have two lobes and formed from unhybridized p orbitals. The electrons are exposed on the outside of the molecule this makes them more extended. In other words, electron can escape from its site and diffuse distant sites. Because of this unlocalization, these structures are much more reactive. Note that in Figure 4.8(b), sigma and pi bonds are in different planes. This type of bonding results in the formation of hexagonal rings, in order to optimize the interactions between the unhybridized p orbitals. When the sp^1 hybridization occurs two carbon atoms bond to each other by one σ bond and two π bonds. The two unhybridized pi orbitals are oriented in the y and z planes (Figure 4.8(c)).

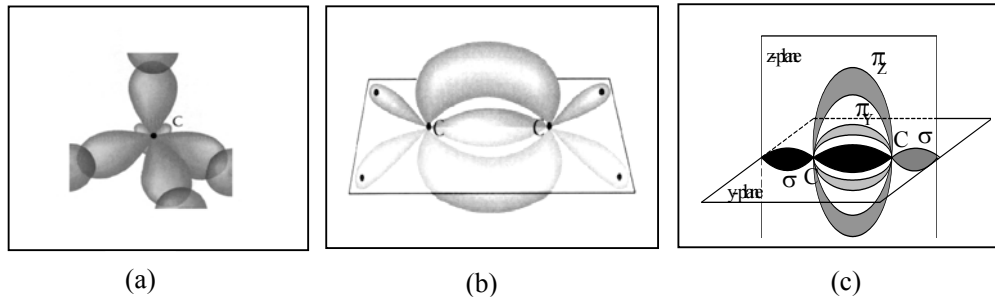


Figure 4.8 Carbon atom bonding structure (a) four σ bonds, (b) carbon atoms are connected by one σ and one π bond, (c) p_y and p_z orbitals form π bonds.

4.2.4 General Structure

Local atomic configuration of amorphous carbon films may be either tetrahedral (sp^3), planar (sp^2) or linear (sp^1) in any ratio depending on the production conditions. Huckel model [22] can be used to calculate the energies of the bonds. Consequently, a-C could be viewed as sp^2 based pi-bonded and sp^3 based sigma-bonded structure. First part is conductive and determines the electrical and optical properties through pi-states constituting the band edge states and the band gap. On the other hand second part is resistive and determines the mechanical properties forming the skeleton of the structure. The pi-bonded structures tend to form clusters to maximize the bonding energy [23]. In Figure 4.9 more or less smaller gaps are the result of the size of the clusters. The optical gap depends on the mean cluster size.

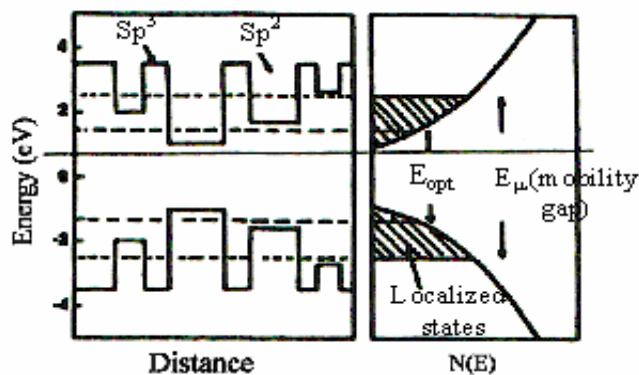


Figure 4.9 Schematic energy band diagram of a-C:H

The mobility gap for a-C, which is formed by the mobility edges, is larger than the optical gap. The mobility gap is determined by the gap of sp^3 boundary regions between π bonded clusters. These larger gaps constitute barriers against the motion of π -electrons, which are confined within the smaller gap islands. The electronic conduction between islands might be by tunneling through the surrounding sp^3 like regions. The mobility edge should depend on the width of these boundary layers. Larger boundaries results in larger mobility gap, and vice versa.

In addition to the bonding structures of a-C, it should be in mind that hydrogenation of the a-C has a tendency of converting sp^2 bonding to sp^3 , by crushing the π bonds. According to Figure 4.10, the π states lie closer to E_f . Therefore hydrogenation is expected to widen the gap by destroying π states associated with sp^2 bonding.

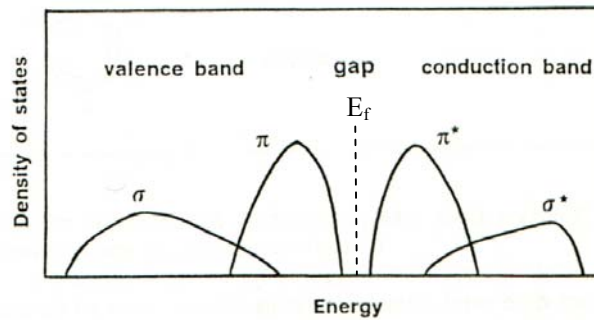


Figure 4.10 Schematic electronic band structure of amorphous carbons

In the following sections optical measurements on amorphous silicon and silicon based amorphous thin films are introduced. Results are evaluated according to the background mostly given in chapter 2 and the plasma events are taken into account at some extent while explaining the effects of carbon content and RF power on film production.

4.3 Delta (Δ) and Psi (Ψ) Simulations in Ellipsometric Measurements

As it is previously stated, when examining a sample with ellipsometer; delta (Δ) and psi (ψ) values are measured by the device. Information about optical constants, thickness (and even the oxide layer thickness and surface micro-roughness) can be obtained by using a suitable physical model on the measured parameters as it is explained in chapter 2 and chapter 3. In this section, some simulated delta (Δ) and psi (ψ) versus angle of incidence curves are examined at single wavelength of 632 nm. as the incidence angle is taken as a variable. First, only one medium is considered, then additional layers are taken into account. The fundamental equation for ellipsometry states that

$$\rho = \tan \psi e^{i\Delta} \quad (4.3)$$

$$\text{where} \quad \psi = \arctan \left| \frac{r_p}{r_s} \right| \quad \text{and} \quad \Delta = \Delta_p - \Delta_s \quad (4.4)$$

According to these definitions and Figure (2.2), ψ must be between 0° and 45° , because the absolute value of r_s is greater than r_p . Furthermore r_p is zero when the angle of incidence equals to Brewster angle (θ_B) in the case of a dielectric sample. Then ψ is zero at that angle. In addition, Δ is equal to 180° for all the angles smaller than θ_B , and 0° for the angles larger than θ_B . Therefore at Brewster angle a sharp decrease from 180° to 0° is expected ideally. On the other hand, For absorbing materials, r_p does not go to zero but to a minimum at an angle known as the pseudo-Brewster angle (Figure 4.11b). In addition, the angle where $\Delta = 90^\circ$ is known as the principal angle (θ_p). Which is known to be very close to the Brewster angle [24]. As the material's absorption characteristic increases, minimum in ψ departs from zero, and the sharp decrease in Δ begins to soften.

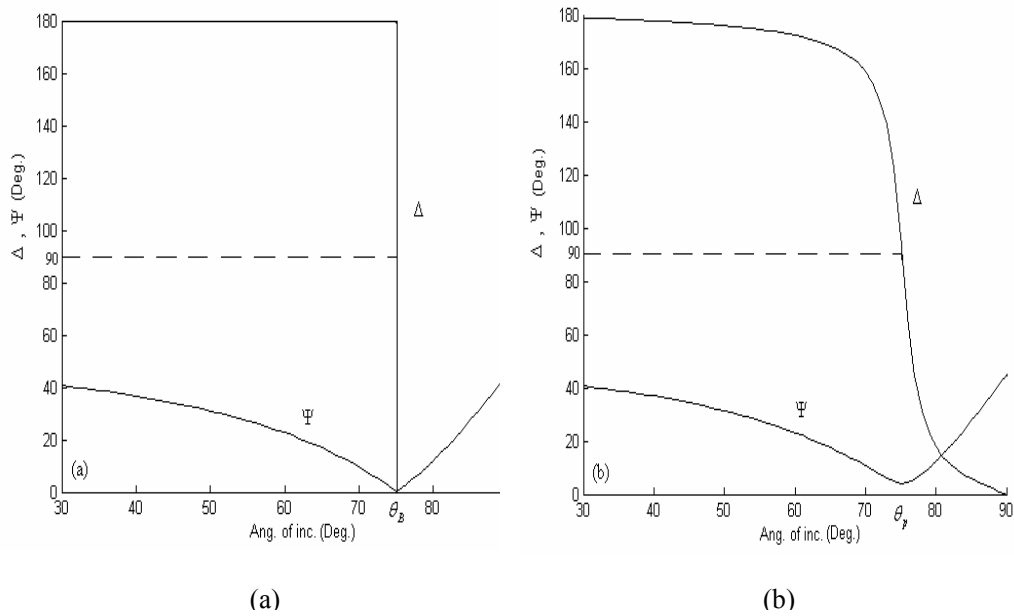


Figure 4.11 Sample del., psi vs angle of incidence curve for (a) ideally non-absorbing, (b) weakly absorbing bulk semiconductor (such as silicon).

When a thin film is taken into account on a bulk medium, the curves are changed. Both the real part (n) and the imaginary part (k) of the refractive index affect the $\Delta - \psi$ vs. angle of incidence curves. Surface roughness and oxide layer may also affect the curves. As an example, if an absorbing film is considered, the general trend is that the value at which the ψ makes minimum is shifted to right and up as the value of k increases (Figure 4.12). Note that, in very small k values this trend may not be obeyed. Apart from that, the effects of the surface roughness and a thin oxide layer are seen to be usually relatively weaker on the delta and psi versus angle of incidence curves. When considering the physical models, these effects are represented by few nanometers and have very slight effect on graphs. Generally ψ minimum is raised and shifts it to the right. And decrease in delta softens and shifts to the right as the above-mentioned defects intensify. Specifically, the oxide layer effect on silicon substrate is also discussed in the following sections. Dust particles, grease and similar effects can not be modelled matematically and they may have great influence on measurements sometimes, as it is examined in the following sections too.

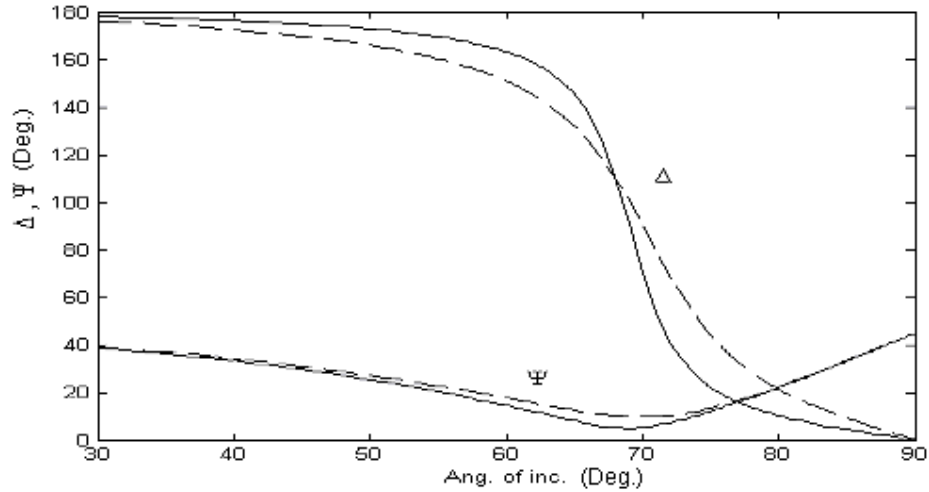


Figure 4.12 Matlab is used to make the simulation. Effect of increasing extinction coefficient is shown. Solid line represents the film with $n=2.6$ and $k=0.4$, while dashed line represents $n = 2.6$ and $k = 0.8$. Thicknesses are 400 nm. Substrates are assumed to be silicon.

4.4 Measurements on Glass Substrate

At the first step some simple experiments are performed on glass substrate with multiple angle of incidence (MAI) ellipsometer at single wavelength of 632 nm in order to find the refractive index by using ellipsometric measurements.

First, the measurement is performed for eight angle of incidence on bare glass (corning type), which is actually an a-Si, without any additional process (Figure 4.13 (a)). Second, a strip of band is stucked to the bottom of the glass slab in order to make the surface rough for reducing multiple reflections from the bottom by causing back-scattering, and the measurement is repeated (Figure 4.13 (b)).

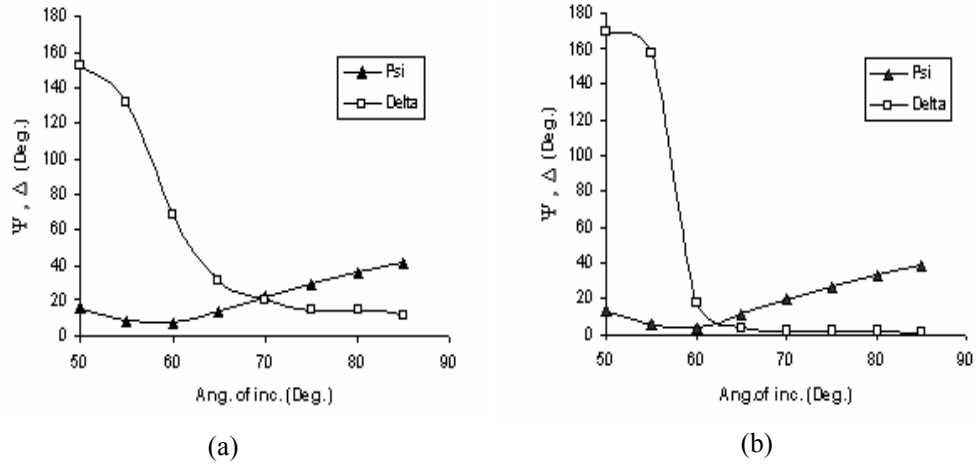


Figure 4.13 Psi and delta versus angle of incidence curves (a) for bare glass, (b) for band-sticked glass.

Absorption is known to be negligible in glass at a wavelength of 632 nm. therefore a comparison of above figures and Figure 4.11 shows that the band-sticked sample is nearer to ideal. In other words, back reflections deteriorate the measurements, therefore should be avoided. Quantitatively, according to the definition of the Brewster's angle from eq. (2.29)

$$\tan \theta_B = \frac{n_{glass}}{n_{air}} \quad (4.3)$$

From data points in Figure 4.13 (b), the minimum in θ_B seems to occur between 55° and 60° . It is roughly estimated as 58° , and taking $n_{air} = 1$, it is found that $n_{glass} = 1.60$ where original value is around 1.52.

For the two samples, refraction coefficients can also be found from eqs. (2.67) and (2.68) for any data point in Figure 4.13 (a) and Figure 4.13 (b).

Calculations are made and the results are shown for the band-sticked sample in table 4.1. The index values for clean back surface are also calculated and it is seen that results are smaller than the band-sticked sample, in the vicinity of 1.45, which is in accordance with Hayton *et al* [25] around the principal angle.

Table 4.1 Index values of corning glass at 632 nm.

Angle	ψ	Δ	n
50°	13.0936	169.9187	1.64
55°	5.6059	157.6295	1.62
60°	3.4279	17.2244	1.59
65°	11.0256	3.7361	1.59
70°	18.9457	1.8857	1.57
75°	26.5592	1.8200	1.54
80°	32.9262	1.8154	1.55
85°	39.0231	1.2857	1.56

The index values calculated from eq. (2.67) and (2.68) are more correct for the band-sticked sample than the other. Calculated k values are very different from one another for the two sample and it is estimated that although the formulae are correct, experimental errors overcome the real k values which are smaller relative to n. In other words, n is less affected from the noises. Then, it can be concluded that small extinction coefficients can not be properly calculated from reflection ellipsometry.

The sensitivity of the ellipsometer depends on the angle of incidence. Thus, the angles of incidence used in an MAI ellipsometer will be those at which the sensitivity is greatest, which is around the principal angle. In literature, it is seen that this has generally led to experiments being carried out in the angular range of between 40° and 80°. (since the ellipsometer is most sensitive at these angles, it is also most sensitive to errors in the setting of the angle of incidence) [24]. Similarly,

in above measurements the most correct values are obtained for the refractive index when the incidence angle is around the principal angle.

4.5 Measurements on Silicon Substrate: Cleanliness effect in ellipsometry

Ellipsometer is known to be very sensitive to surface conditions such as very thin oxide layer, dust particles, micro roughness effects originating from the atomic structure. The following experiment demonstrates the cleanliness effects on measurements in ellipsometry.

Measurements are made on a p-type silicon wafer substrate with the MAI ellipsometer at single wavelength of 632 nm. First, a measurement is performed on a dirty wafer with various contaminants such as grease, dust and natural oxide on its surface (Figure 4.14(a)). Then, the sample is boiled for 5 minutes in trichloroethylene solution and rinsed in ultrasonically agitated deionized water for 5 minutes (water with high resistivity) to remove grease and dust and it is measured again (Figure 4.14(b)). The same cleaning procedure is done on the wafer before the third measurement is made (Figure 4.14(c)).

The effect of removing the dirt such as grease and dust is apparent from the Figure 4.14. The principal angles and Brewster angles are seen to shift right. Index of refraction is found from the Brewster angle method discussed above. According to that, the measured index of refraction in the first case from Figure 4.14(a) is 1.11, in the second case, from Figure 4.14(b), it is 2.14 approaching to ideal which is between 3.70 - 3.90. Finally, at the last measurement on doubly-cleaned material the index is calculated as 3.73 from Figure 4.14(c).

After these processes, the eventual oxide layer is attempted to be removed by dipping in deionized water-HF solution (diluted HF) with 10:1 volume ratio for 15 seconds at room temperature and rinsed in deionized water.

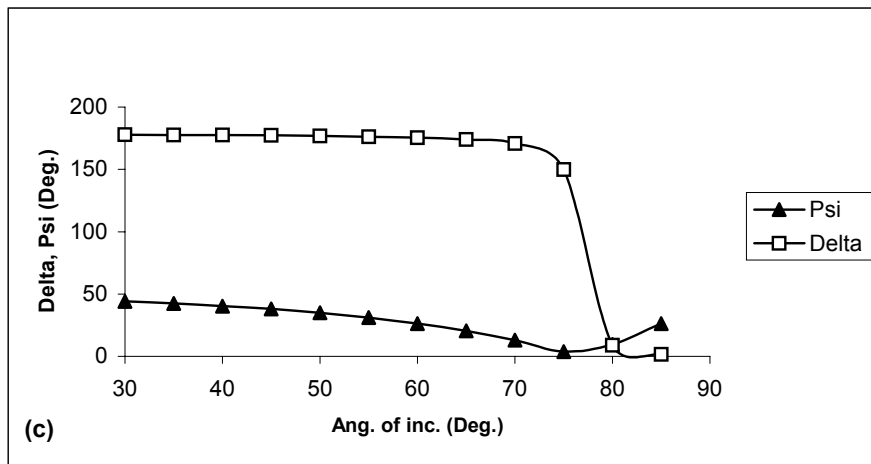
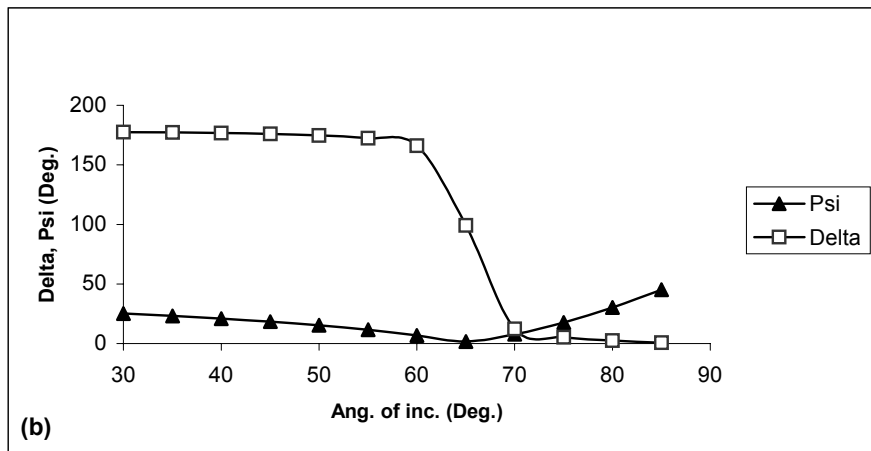
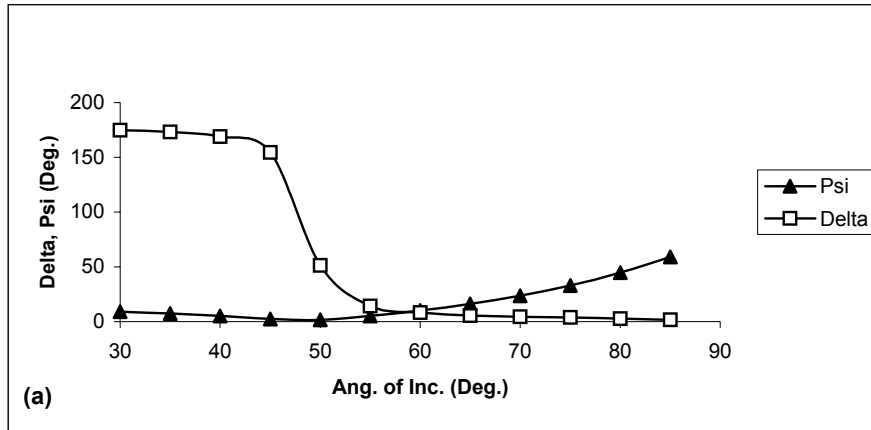


Figure 4.14 Delta and Psi versus Angle of incidence for silicon slab obtained from (a) First measurement, (b) Second measurement. A cleaning procedure is applied before measurement. (c) third measurement. Double cleaning procedure is applied before.

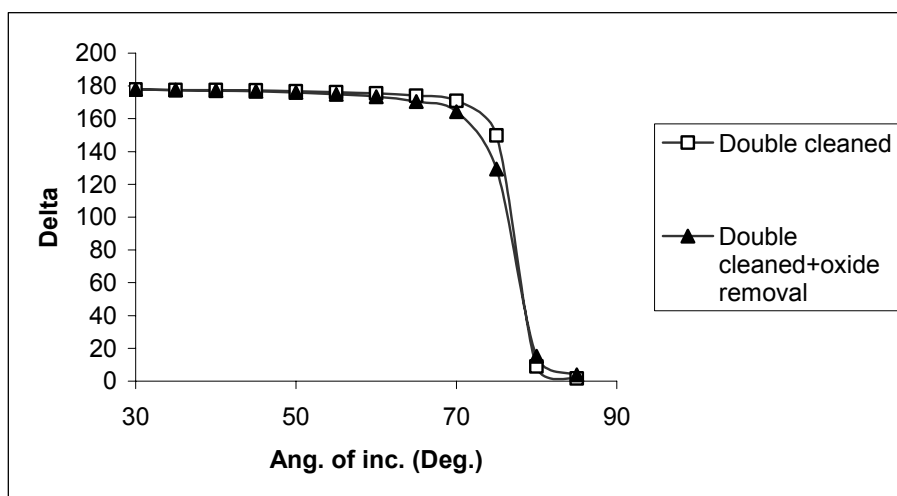


Figure 4.15 Comparison of the delta vs Angle of incidence curves for double-cleaned and double-cleaned + oxide free silicon. The change in psi is indistinguishable, therefore it is not shown in the graph.

As it is seen from the Figure 4.15, the effect of oxide removal causes reverse effect. The decrease in delta softens. From the discussions in section 4.3, this is an unexpected result. It is thought that, this might be brought about by the HF effect which produces surface roughness during etching of the oxide layer from the surface. Theoretical roughness thickness must be larger than the oxide layer (approximately 8-10 Angströms).

This systematic study shows the effect of cleanliness on ellipsometric measurements. One additional point is that, although in glass measurements no additional processes are applied to make the material cleaner, a result with a relatively lower error is found compared to the silicon substrate. This may be due to the surface dirt that show similarity to glass in refractive indices. Of course, a measurement on cleaner glass would possibly give a more accurate value than the one previously given, although not very different.

4.6 Optical Measurements on a-Si_{1-x}C_x:H Thin Films

4.6.1 Production of a-Si_{1-x}C_x:H Thin Films

a-Si_{1-x}C_x:H thin films are deposited on the grounded bottom electrode of a parallel plate PECVD system at 13.56 MHz (Plasma lab μ P 80), (see Figures 4.16 and 4.17). Corning 7059 glasses are used as substrates for ultraviolet-visible optical analysis, respectively. These substrates are dipped in isopropil alcohol for 5 min., rinsed ultrasonically agitated in deionized water (DIW) for 10 min. and then heated at 120°C for 5 minutes just prior to deposition.

After the cleaning process, they are loaded into the deposition system as quick as possible. The reactor was pumped down to a base pressure below 1 mtorr and the temperature of the bottom electrode was adjusted to 250°C before letting flow of 50 ccm H₂ in order to clean the system by applying plasma power of 100 mW/cm² under the pressure of 0.5 torr for 5 min. The total source gas flow rate (F), hydrogen flow rate and the pressure are adjusted to values of 20 ccm, 200 ccm (corresponding to a H dilution ratio of 91%) and 0.5 torr, respectively, growth process is started by applying rf power of 30 or 90 mW/cm² as given in Table 4.2 Ethylene (C₂H₄) and silane (SiH₄) are used as source gases and their flow rates F(C₂H₄) and F(SiH₄), respectively, are given in table 4.2 where relative C₂H₄ concentration is defined by $M(C_2H_4) = \frac{[C_2H_4]}{[C_2H_4] + [SiH_4]}$.

Table 4.2 Eight different depositions under a pressure of 0.5 Torr at substrate temperature of 250 °C for the following deposition parameters such as relative C₂H₄ concentration (M(C₂H₄)), SiH₄ (F(SiH₄)) and C₂H₄ (F(C₂H₄)) flow rates and power density (P). The letters “lp” and “hp” denote films grown at low and high powers, respectively. Carbon content increases as the sample number increases. Also the deposition times and x value for the a-Si_{1-x}C_x:H are shown.

Sample	M(C ₂ H ₄)	F(SiH ₄) [ccm]	F(C ₂ H ₄)[ccm]	P(mW/cm ²)	t(min)	x
0lp	0	20	0	30	60	0
0hp	0	20	0	90	72	0
2lp	0.2	16	4	30	132	0.19
2hp	0.2	16	4	90	67	0.19
5lp	0.5	10	10	30	137	0.34
5hp	0.5	10	10	90	90	0.38
7lp	0.7	6	14	30	188	0.45
7hp	0.7	6	14	90	100	0.54

As the ethylene concentration increases, the carbon content of the growing film increases as it is seen from the table 4.2.

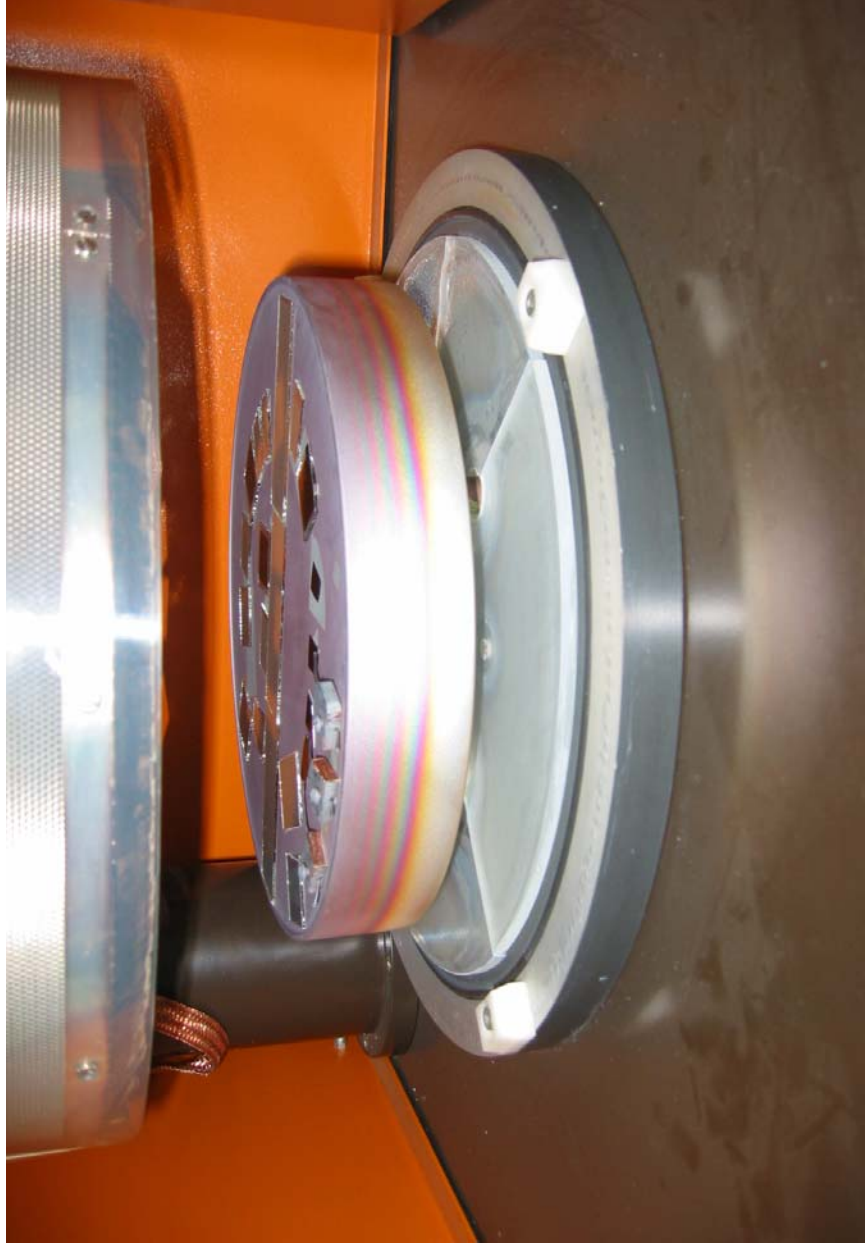


Figure 4.16 A series of glass substrates lying on the bottom grounded electrode of PECVD reactor.

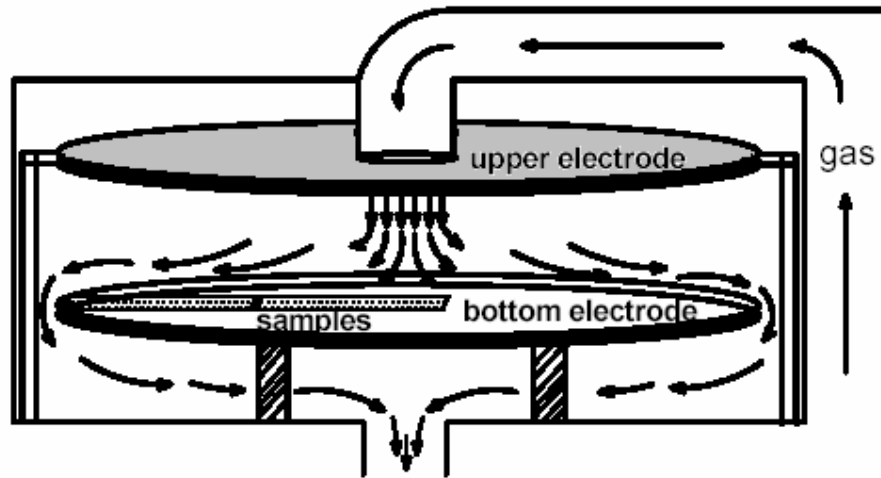


Figure 4.17 Sketch of gas streamlines in the PECVD reactor. Film substrates are lying on the bottom grounded electrode of radius 12 cm. [13].

4.6.2 Expected Reactions in the Plasma Medium

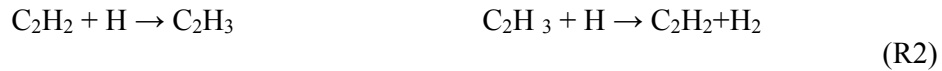
In the deposition of hydrogenated amorphous silicon carbide ($a\text{-Si}_{1-x}\text{C}_x\text{:H}$) thin films, the plasma enhanced chemical vapor deposition method (PECVD) is preferred. Ethylene (C_2H_4) and silane (SiH_4) are used mainly as source gases of carbon and silicon respectively. The properties of material, such as optical band gap, refractive index are determined by the hydrocarbon gas concentration (C_2H_4) or carbon content in the deposited film. Therefore, optical band gap of $a\text{-Si}_{1-x}\text{C}_x\text{:H}$ can be adjusted to any value in the visible range of energy spectrum by changing the hydrocarbon concentration in the process. This property makes this material suitable for LED fabrication. It is useful to summarize the possible reaction mechanisms such as ethylene and silane reactions in the formation of $a\text{-Si}_{1-x}\text{C}_x\text{:H}$ films.

Ethylene (C_2H_4) Reactions:

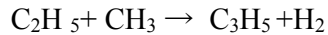
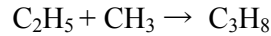
The electrons in the plasma environment initiate the reactions by colliding the C_2H_4 molecules [13].



Because of its higher mobility, the reactions with H atoms becomes significant in the plasma medium. These are listed as,



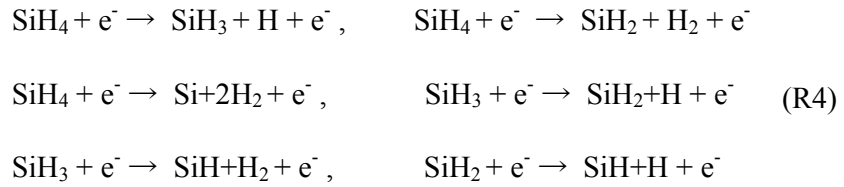
CH₃ have small reaction speed and small sticking coefficient on the surface of growing film. Therefore CH₃ molecules dominate the plasma atmosphere by the following reactions.



If these radicals collide with ethylene (C₂H₄) or acetylene (C₂H₂) molecules, radicals with more hydrogen can be formed. Consequently, polymerization in gas phase might be initiated leading to the formation of dusts; if these dusts stick on the growing film surface, the film becomes structurally more disordered. The species, responsible for deposition of the film, are C₂H, C₂H₃ and C₂H₅ radicals. While they are reacting with the film or substrate surface, they lose some of their hydrogen atoms. But, it's known that a considerable amount of hydrogen stays in the deposited film.

Silane (SiH₄) reactions:

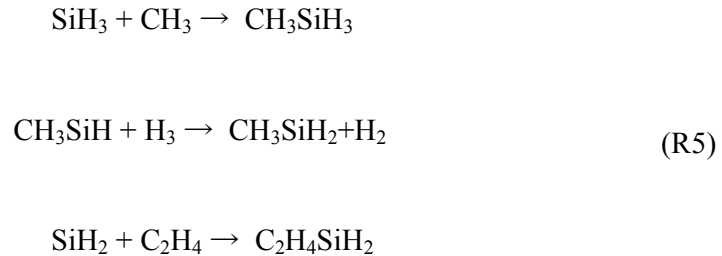
The primary reactions between the electrons and the silane molecules can be given as follows,



During, the deposition of hydrogenated amorphous silicon, all the radicals contained in the plasma cloud contribute to the deposition, but the SiH₃, which is very dense, is the dominant radical in this process. The radicals reaching the substrate or film, are adsorbed at the surface and then connected to the film. SiH₃ may diffuse over the surface for a suitable site and then a hydrogen molecule is desorbed from the surface Si-H bond, leaving behind a silicon dangling bond. Another SiH₃ radical may be subsequently physisorbed (with weak van der waals bond) and diffuses on the surface and then chemisorbed (with covalent bond) by an already created Si dangling bond on the surface.

Deposition of a-Si_{1-x}C_x:H thin films:

In addition to the reactions of previously outlined deposition mechanisms of a-Si:H and a-C:H films separately, when SiH₄ and C₂H₄ source gases are introduced into the plasma medium, the new radicals formed because both gases might start to react with each other. Possible reactions may be outlined as



4.6.3 Optical Experiments

The preparation of the samples are summarized above. These samples are examined with both MAI ellipsometer at 632 nm. and uv-vis transmission spectrometer whose incident wavelength is between 1100 nm. and 200 nm. In both ellipsometry and transmission spectroscopy, data are taken from the samples at multiple points in radial direction, starting from the edge of the reactor to the middle.

In spectroscopic analysis, Swanepoel's method and numerical fitting techniques (optichar. program) are used to handle the data. From the former, the thickness values can be calculated. But index values are only found at different wavelengths, therefore another evaluation is needed. Numerical techniques are exploited by using the initial thickness values found from the former method. From the numerical techniques, thicknesses and deposition rates, refraction indices, and absorption coefficients are found. Additionally, optical gaps E_{04} and E_g are calculated by using absorption coefficients.

Ellipsometer results are examined according to numerical fitting techniques, refraction indices and thicknesses are found.

4.6.4 Discussions

Some observations can be made from the figures. First of all, it is seen that the thickness values found from Swanepoel's method and numerical fitting techniques are in agreement (Figure 4.18). Except for the sample 0lp, which is essentially an a-Si:H. This may result from the fact that, absorption starts at greater wavelengths in that sample (also it is apparent from the E_g graphs (Figure 4.21); as the carbon content decreases, energy values decrease which corresponds to higher wavelengths). It makes data acquisition hard for Swanepoel method. 0hp doesn't show a similar character, because its thickness is greater than the other and the

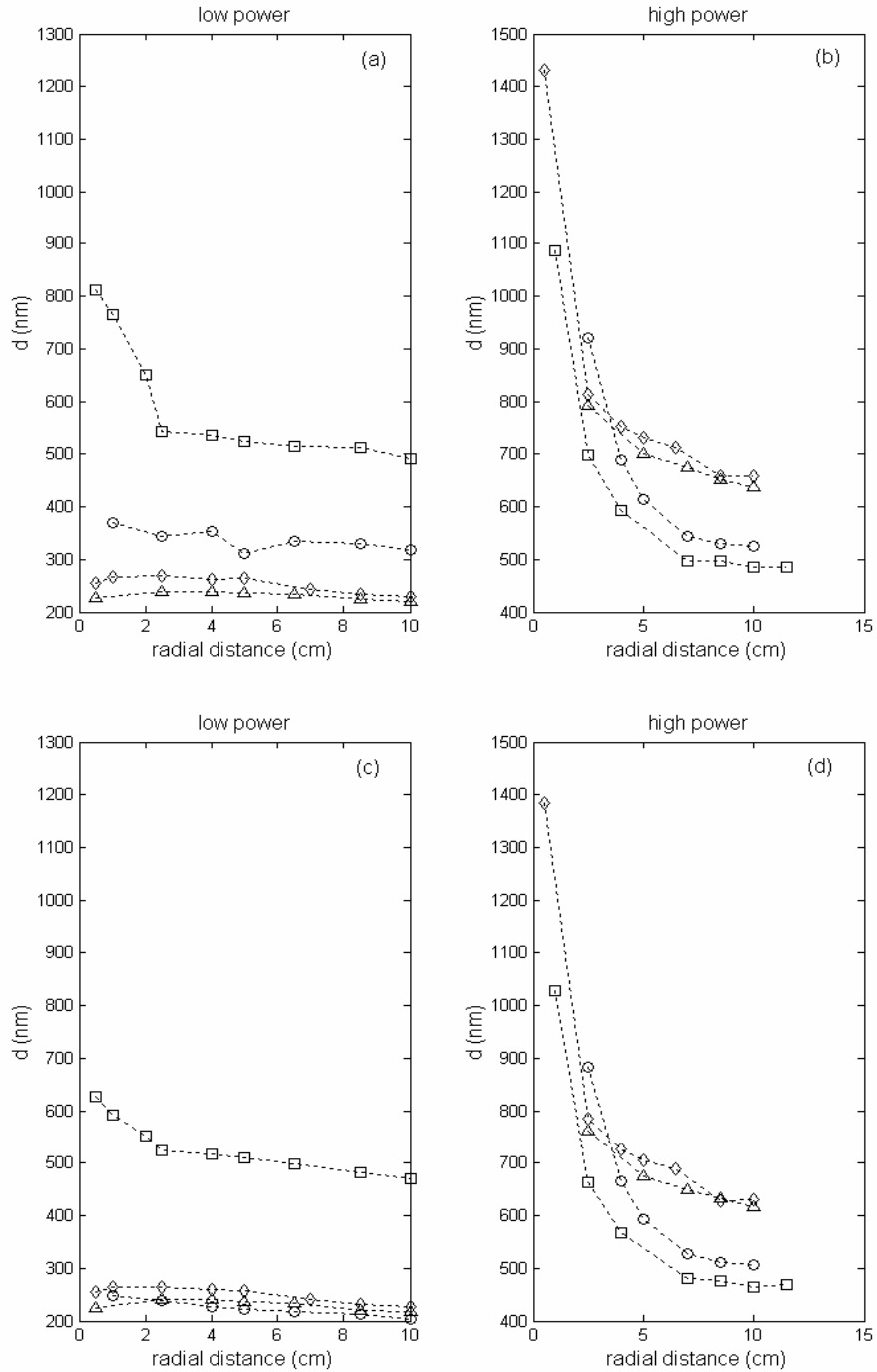


Figure 4.18 Thickness values from transmittance found by (a) Using the method of Swanepoel for low power. (b) Using the method of Swanepoel for high power. (c) Using numerical techniques for low power and (d) Using numerical techniques for high power. Note that, circles, squares, triangles and diamonds, correspond to increasing carbon contents, respectively. Radial distance of about 0 cm corresponds to the edge of the bottom electrode whereas that of about 11.5 cm corresponds to the center of the electrode.

Swanepoel method gives more accurate values for thick films because of the interference fringes which exist more for a thick film than the thin one.

Figure 4.18 shows the thickness variations along the radial direction for each of the eight different $a\text{-Si}_{1-x}\text{C}_x\text{H}$ films evaluated by two approaches. One could not say that there is always a perfect uniformity of thickness. Especially, films, deposited at high power ($90\text{mW}/\text{cm}^2$) exhibit drastic thickness non-uniformities (Figure 4.18b - 4.18d). However; for the films grown at lower power ($30\text{mW}/\text{cm}^2$), the thickness uniformity is achieved within acceptable experimental fluctuations (Figures 4.18a and 4.18c).

Deposition rates are calculated by dividing the thicknesses found from numerical techniques by the deposition times. Physically, it is the deposition rates rather than the thicknesses that are important.

Figure 4.19 presents the deposition rates of eight films. In this frame, the degree of film uniformity is clearer. Let us analyze the low power films (Figure 4.19a). There is a substantial difference between carbon rich films (shown by triangle and diamond symbols) and silicon rich films (shown by circle and square symbols). For carbon rich films, the growth rate is very slightly increasing along the radial direction (from the center to the edge). As for the silicon rich films, the growth rate is 2.5 times larger than the previous ones. Moreover, a distinguishable non-uniformity exists (although very slight along most of the range, it is accentuated towards the electrode edge).

The large growth rate of silicon rich films is probably due to the abundance of SiH_3 radicals. (see reaction R4 in section 4.6.2) since this radical being less reactive with other species in plasma medium, it can have largest lifetime (or residence time) and thus it may have the largest probability to reach the growing film surface. As the source gasses are supplied to the middle region of the reactor, the concentration of SiH_3 , as reaction by product, must be increasing towards the electrode edge, due to longer occurrence time.

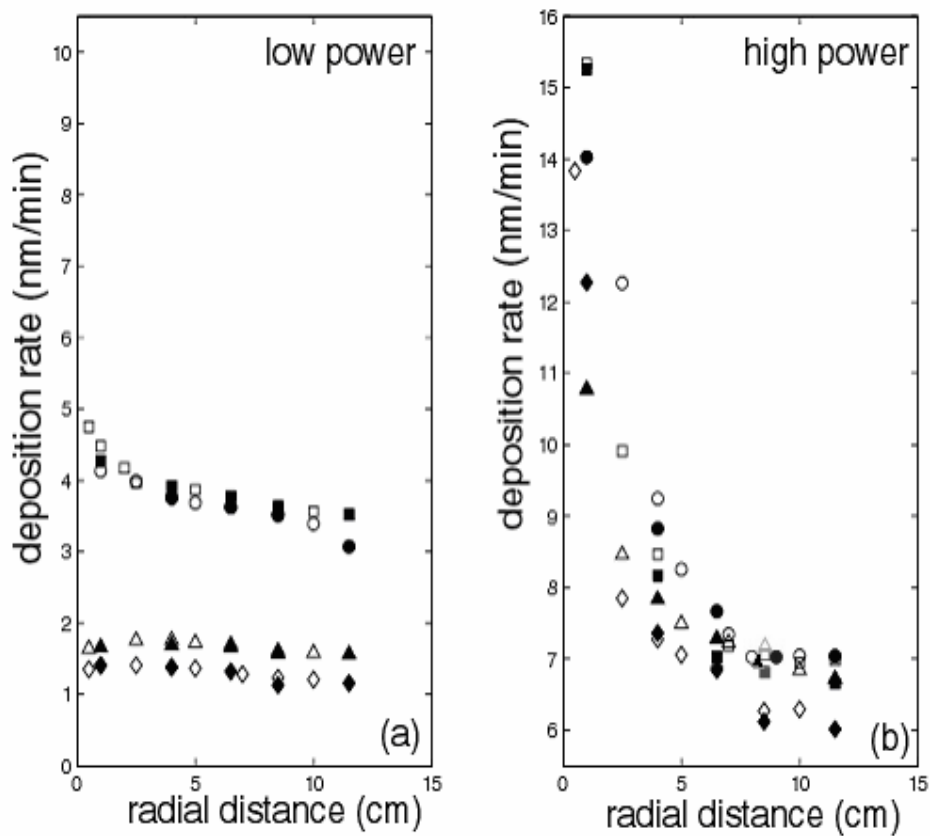


Figure 4.19 (a) Deposition rates, obtained from transmittance (empty markers) and ellipsometry (full markers) measurements, of samples 0lp, 2lp, 5lp and 7lp, denoted by circles, squares, triangles and diamonds, respectively. (b) Deposition rates, obtained from transmittance (empty markers) and ellipsometry (full markers) measurements, of samples 0hp, 2hp, 5hp and 7hp, denoted by circles, squares, triangles and diamonds, respectively. Radial distance of about 0 cm corresponds to the edge of the bottom electrode whereas that of about 11.5 cm corresponds to the center of the electrode.

This increase in concentration towards the electrode edge may be behind the slight increase in the growth rate [26]. An efficient incorporation of SiH_3 radical to the growing surface, is expected to be proportional to the silicon dangling bond (DB) density on the growing surface. Nevertheless the growing surface must be covered by hydrogen, in other words, the dangling bonds are saturated or passivated by hydrogen. This fact, in turn, might impede the film growth. In this respect, subsidiary mechanisms should exist to remove these bonded hydrogen to have available dangling bonds for binding SiH_3 radical [27,28]. Moreover the incorporation of SiH_3 to the film surface would bring about 75% H content of the resulted film; but experimental measurements point out that a-Si:H films contain seriously less hydrogen (between 10-20 %). This substantial difference requires the desorption (or release) of hydrogen during the microscopic growth mechanism. [29]. This mechanism should exist since experiments show that SiH_3 has a very large sticking coefficient on the growing surface. A reasonable mechanism might be two step bonding of SiH_3 radical, i.e, in a first step SiH_3 reacts with Si-H bond at the surface, producing SiH_4 (silane molecule) which is released from the surface into the gas medium, leaving behind a silicon dangling bond. In the following step, a new SiH_3 radical is bound definitely to this dangling bond. Besides, a parallel ionic bombardment of the growing surface helps to remove surface hydrogen, by the way increases the density of dangling bonds. And enhances the surface reaction of SiH_3 radical. This last mechanism might explain the rising growth rate towards electrode edge since relatively higher voltage towards electrode edge might increase the plasma density and ion density. This intensified ionic bombardment together with the higher concentration of SiH_3 radicals raise the growth rate (Figure 4.19a) [30,31]. As for carbon rich films (Figure 4.19a), the growth rates are substantially reduced. In this case, the film surface might be covered by hydrogen bound to both Si and C sites; the removal of hydrogen from C-H sites is less probable since C being more electronegative, binds more strongly hydrogen, and leads to lower density of dangling bonds which directly reduces the growth rates.

Moreover, the growth of carbon rich films could not be explained by a single precursor radical; instead a wide varieties of radicals, ions and their combinations

together with the ionic impinging physical and chemical effects on the surface are influential in the growth rate [32]. One can speculate about the carbon based radicals involving in the growth, i.e, unsaturated species such as C_2H , C_2H_3 , C_3H_5 rather than saturated radicals such as CH_3 , C_2H_5 (see reaction R1 in section 4.6.2) should be more reactive on the film surface due to their π orbitals. The carbon based radicals reacting with SiH_3 radical reduce the contribution of the latter to the growth. Although details of surface reactions are not yet well known, a large amount of hydrogen desorption as reaction by-products might be foreseeable. In spite of this expected release of hydrogen, a relatively large amount of hydrogen remains in the films, affecting their properties [33,34,35]. On the other hand, the sticking coefficients of the above mentioned carbon based radicals are very low, leading to a slow growth rate.

High power produces a few times larger growth rates compared to the ones deposited at low power (see Figure 4.19b). At this high power, the effect of the carbon content on the growth rate remains within the experimental fluctuations. In other words, high power is much more effective to produce carbon based radicals, reaching the level of silicon based radicals. As the concentration of radicals increases towards the electrode edge (together with the previously mentioned higher plasma density due to larger voltage), the growth rates rise drastically towards the electrode edge, and an unacceptable film thickness inhomogeneity results. (Figure 4.19b). Also ion bombardment effect may be efficient in the increase of deposition rates.

Figure 4.20 shows the radial distributions of the refractive indices determined by both the ellipsometry and transmission spectroscopy. These results show that the refractive index of films may be adjusted between the values 4.1 - 2.2 by changing only the carbon content. This is extremely important for the application point of view. Although little radial uniformity exists for low power films (within experimental fluctuations), a nonuniformity exists at high power ones. This radial inhomogeneity in refractive index at high ethylene concentration at high power points out that along the radial direction, the carbon content of a film

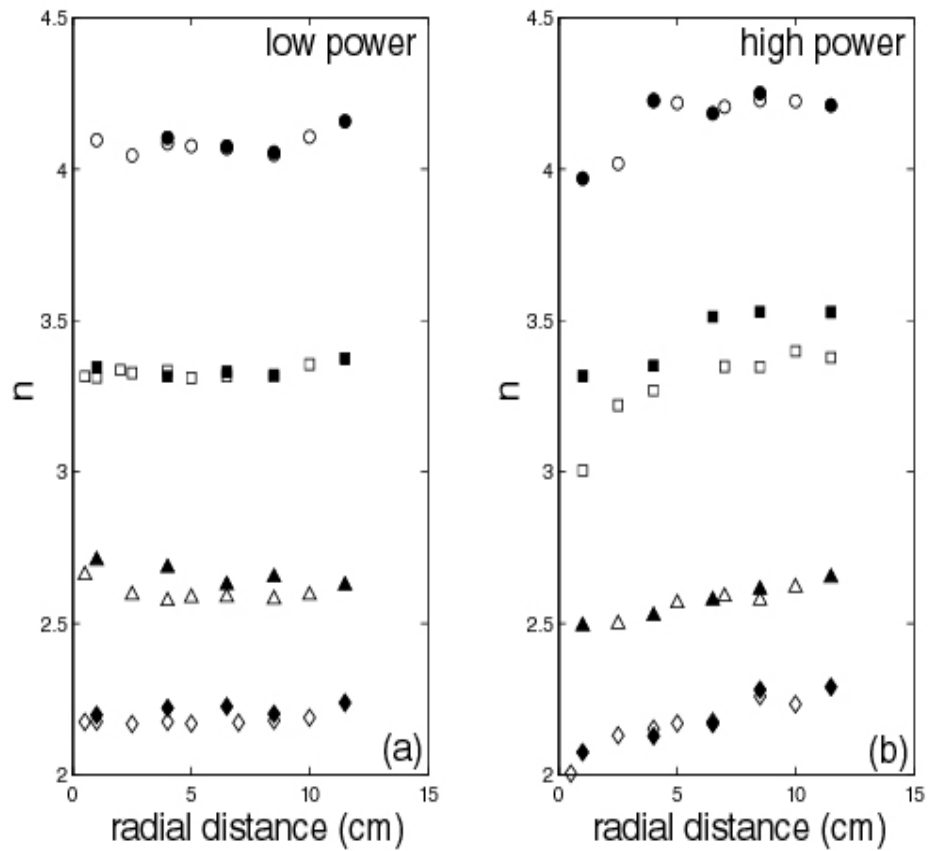


Figure 4.20 (a) Refractive indices, obtained from transmittance (empty markers) and ellipsometry (full markers) measurements, of samples 0lp, 2lp, 5lp and 7lp, denoted by circles, squares, triangles and diamonds, respectively. (b) Refractive indices, obtained from transmittance (empty markers) and ellipsometry (full markers) measurements, of samples 0hp, 2hp, 5hp and 7hp, denoted by circles, squares, triangles and diamonds, respectively. Radial distance of about 0 cm corresponds to the edge of the bottom electrode whereas that of about 11.5 cm corresponds to the center of the electrode.

increases towards the electrode edge. The reason is that, because electronegativity of carbon is greater than the electronegativity of silicon, Si-C σ bonds are stronger than the Si-Si σ bonds. That should cause lower refractive indices [36] as the carbon content and Si-C bonds increase towards the electrode edge. As previously discussed, this is expectable since towards the electrode edge, the concentration of carbon based radical might be seriously increased. Variations in refractive indices for high power are in agreement with Ambrosone *et al* [37].

E_g and E_{04} are shown in Figure 4.21. As the carbon content increases, energy gaps increase for all samples. In low power a uniformity is observed, while a small decrease occurs in high power in the radial direction from the edge to the center. At that point, the relationship between the graphs of indices and energy gaps should be emphasized; energy gaps are inversely proportional to indices. Therefore, gaps can be adjusted by carbon concentration. From the graphs, it is seen that the energy values are in the visible range. Lastly, E_{04} versus carbon concentration graphs are drawn (Figure 4.22) and it is seen that they are in accordance with the literature [37,38]. In summary, the carbon content may be used as modulation parameter of the optical gap almost along the whole visible range.

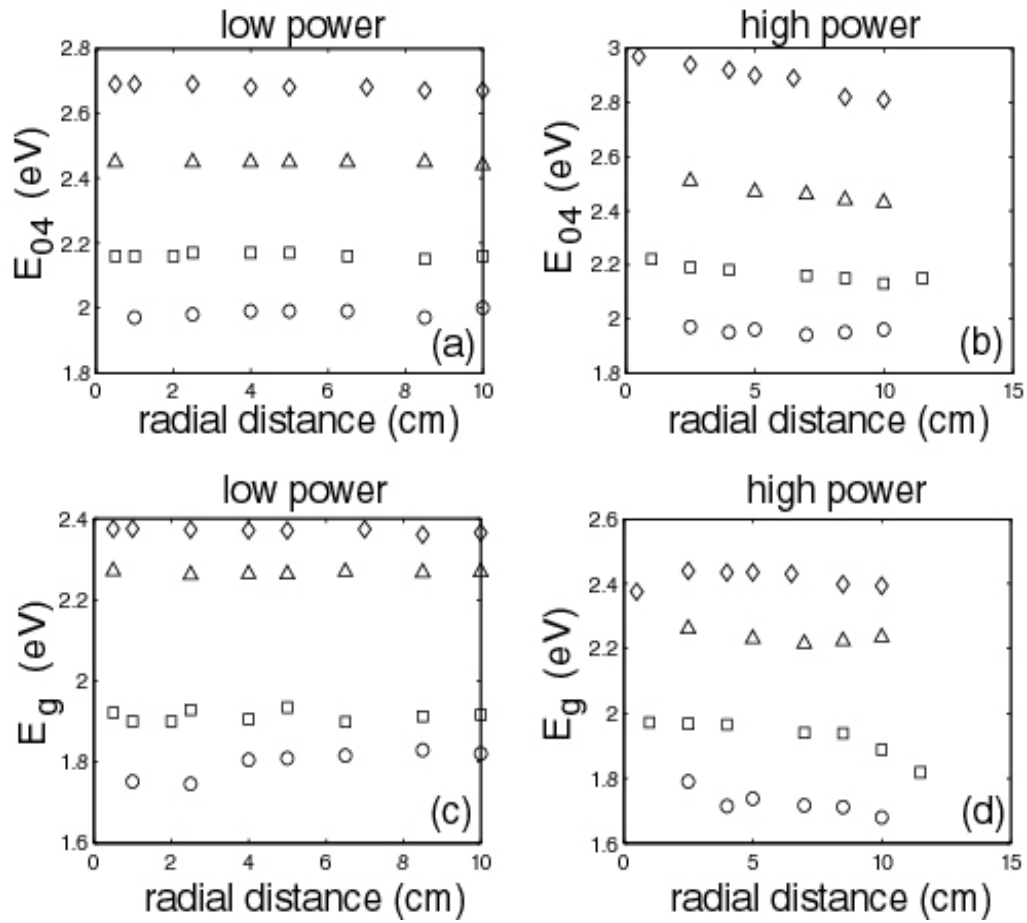


Figure 4.21 E_{04} values as a function of radial distance of the bottom electrode, obtained from transmittance measurements of films (a) 0lp, 2lp, 5lp and 7lp, denoted by circles, squares, triangles and diamonds, respectively. (b) 0hp, 2hp, 5hp and 7hp, denoted by circles, squares, triangles and diamonds, respectively. Optical gaps E_g as a function of radial distance of the bottom electrode obtained from transmittance measurements of films (c) 0lp, 2lp, 5lp and 7lp, denoted by circles, squares, triangles and diamonds, respectively and (d) 0hp, 2hp, 5hp and 7hp, denoted by circles, squares, triangles and diamonds, respectively. Radial distance of about 0 cm corresponds to the edge of the bottom electrode whereas that of about 11.5 cm corresponds to the center of the electrode.

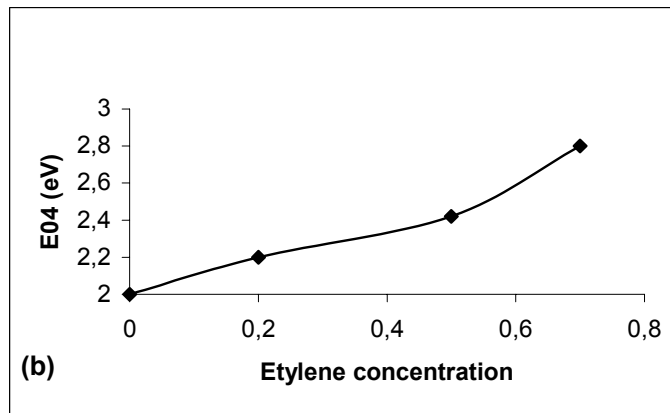
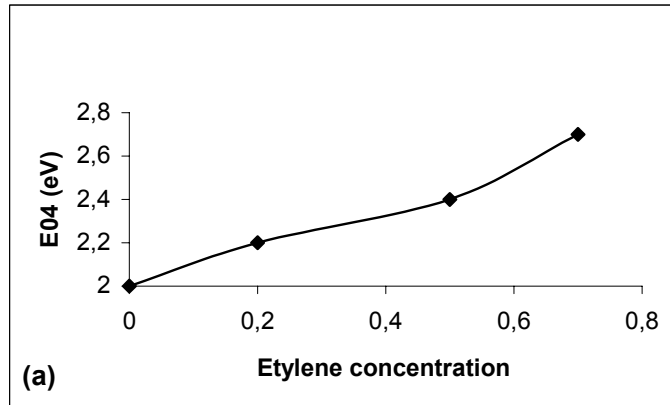


Figure 4.22 E_{04} versus carbon content for (a) low power (b) high power for the same position in the reactor which is 10 cm from the edge.

CHAPTER 5

CONCLUSION

In this study, the aim is to use systematically the single wavelength ellipsometer for analyzing thin solid films. A parallel analysis by visible spectrometer has been achieved in order to qualify and test the ellipsometric measurements.

Within the frame of light-solid medium interaction, the basic concepts and expressions of the electromagnetic waves have been resumed in order to establish the basic ellipsometric equations in terms of Fresnel coefficients. Parallely, the expression of light transmission have been outlined.

A capacitive type plasma enhanced chemical vapour deposition (PECVD) system and its surrounding practical and theoretical principles are presented. This system has been succesfully used to grow a-Si_{1-x}C_x:H thin films on glass substrates. Before analyzing these films, the optimum conditions of ellipsometric measurements have been determined. In this respect, first the effect of back reflection has been carried out, and it has been corrected. The eventual effects of surface dirts, contaminated surface layer (such SiO_x) and surface roughness have been studied. The microscopic structure of a-Si_{1-x}C_x:H film has been discussed.

A series of a-Si_{1-x}C_x:H films with increasing carbon content at two different powers has been deposited. Serious inhomogeneities in growth rates, refractive indices and optical gaps along the radial direction of bottom electrode (sample electrode) have been assessed for high power. An acceptable radial uniformity in

all the above cited film parameters has been obtained at low power even if the growth rate has been substantially reduced.

Finally, this work has showed irrefutably that the refractive index (from about 4 to about 2) and optical gap (along the whole visible range) may be adjusted as a practical requirement of optoelectronic applications.

REFERENCES

- [1] L. Sansonnens, A. Pletzer, D. Magni, A. A. Howling, Ch. Hollenstein and J. P. M. Schmitt, *Plasma Sources Sci. Technol.*, vol. 6 (1997), p.178.
- [2] J.R. Reitz, F.J.Milford, R.W.Christy, *Foundations of Electromagnetic Theory*, Addison-Wesley Publishing, (1992), p. 394.
- [3] F.L. Pedrotti, S.J., L.S. Pedrotti, *Introduction to Optics*, 2nd ed. Prentice Hall, (1996)
- [4] R. Swanepoel, *J. Phys.E: Sci.Instrum.*, Vol. 16 (1983), p.1214.
- [5] B. Akaoglu, I. Atilgan, B. Katircioğlu, *Applied Optics*, Vol. 39, No. 10, (2000), p.1611.
- [6] M. Born, E. Wolf, *Principles of Optics*, 3rd ed. Pergamon Press, (1965).
- [7] T.S. Chao, C.L. Lee, T.F. Lei, *J.Electrochem. Soc.*, Vol. 138, No.6 (1991) p. 1756.
- [8] R.M.A. Azzam, N.M. Bashara, *Ellipsometry and Polarized Light*, North Holland, Amsterdam, (1989).
- [9] Ph.J. Roussel, J. Vanhellefont, H.E.Maes, *Thin Solid Films*, Vol. 234 (1993), p.423.
- [10] H. Conrads, M. Schmit, *Plasma Sources Sci. Technol.*, vol. 9(2000), p. 441.
- [11] W. J. Goedheer, *Plasma Sources Sci. Technol.*, vol. 9 (2000), p.507.
- [12] N. St. J. Braithwaite, *Plasma Sources Sci. Technol.*, vol.9 (2000), p.517.
- [13] Barış Akaoglu, Ph.D. Thesis, Middle East Technical University, 2004.
- [14] V.S. Nguyen, in: *Handbook of Thin-Film Deposition Processes and Techniques*, ed. by K.K. Schuegraf, Noyes Publications, William Andrew Publishing, New York (1988).
- [15] İ. Atilgan, Ph.D. Thesis, Middle East Technical University, 1993.
- [16] *Lambda 2 UV/VIS Spectrometer Operator's Manual*, Bodenseewerk Perkin-Elmer GmbH, 1990.
- [17] H.G.Tompkins, *A user's Guide to Ellipsometry*, Academic Press, (1993), p. 21.

- [18] K. H. Zaininger, A. G. Revesz, RCA Laboratories, 1964, p.85.
- [19] EL X-02C High Precision Ellipsometer's Installation Manual, 1998
- [20] D. E. Sweenor, S. K. O'Leary, B. E. Foutz, Solid State Communications, Vol. 110 (1999), p. 281–286.
- [21] J. Tauc, R. Grigorovici, A. Vancu, Phys. Stat. Sol., Vol. 15 (1966), p. 627.
- [22] Kıvanç Sel, M.S. Thesis, Middle East Technical University, 2002
- [23] J. Robertson, E.P. O'Reilly, Physical Review B, Vol. 35 (1987), p.2946
- [24] T.E. Jenkins, J. Phys. D: Appl. Phys. 32 (1999), p. R45–R56.
- [25] D. J. Hayton, T. E. Jenkins, Meas. Sci. Technol. Vol. 15 (2004), p. N17–N20.
- [26] A. Roth, F.J. Comes, W. Beyer, Thin Solid Films, vol. 293 (1997), p. 83.
- [27] A. von Keudell, Plasma Sources Sci. Technol., vol. 9 (2000), p. 455.
- [28] J. Robertson, M.J. Powell, Thin Solid Films, vol. 337 (1999), p. 32.
- [29] W.M.M. Kessels, A.H.M. Smets, D.C. Marra, E.S. Aydil, D.C. Schram, M.C.M. van de Sanden, Thin Solid Films, vol. 383 (2001), p.154.
- [30] J.C. Knights, R.A. Lujan, M.P. Rosenblum, R.A. Street, D.K. Biegelsen, J.A.Reimer, Appl. Phys. Lett., vol. 38 (1981), p. 331
- [31] F.J. Kampas, J. Appl. Phys., vol. 53 (1982), p.6408.188 B
- [32] A. von Keudell, W. Jacob, J. Appl. Phys, vol. 79 (1996), p. 1092.
- [33] F. Giorgis, C.F. Pirri, E. Tresso, P. Rava, Philosophical Magazine B, vol. 75 (1997), p. 471.
- [34] J. Robertson, J. Non-Crystalline Solids, vol. 137-138 (1991), p. 825.
- [35] M. Koos, Diamond and Related Materials, vol. 8 (1999), p. 1919.
- [36] B. Akaoglu, İ. Atılgan, B. Katırcıoğlu, Thin Solid Films, Vol. 437 (2003) p. 257-265.
- [37] G. Ambrosone, U. Coscia, S. Ferrero, F. Giorgis, P. Mandracci and C. F. Piri, Philosophical Magazine, B, 2002, Vol. 82, No. 1, p. 35-46.]
- [38] V. Chu, J. P. Conde, J. Jarego, P. Brogueira, and J. Rodriguez, N. Barradas, J. C. Soares. J. Appl. Phys. 78 (5), 1995.